Journal of
Nuclear Engineering

MDPI

Article

A Novel Multi-Point Depletion Model for Molten Salt Reactors

Mohamed H. Elhareef [†] **and Zeyun Wu** [*]

Department of Mechanical and Nuclear Engineering, Virginia Commonwealth University, Richmond, VA 23284, USA
* Correspondence: zwu@vcu.edu
† Current address: Department of Nuclear Engineering, Texas A&M University, College Station, TX 77843, USA.

Abstract

Molten Salt Reactors (MSRs) offer significant advantages over conventional reactors but introduce unique modeling challenges due to their circulating liquid fuel and strong coupling among nuclear, chemical, and fluid transport processes. These challenges are amplified in depletion calculations, where MSR specific phenomena such as online refueling, off-gas removal, material redistribution, and other flow driven processes must be accurately represented. This work presents a novel multi-point depletion model that efficiently and accurately predicts isotopic evolution in MSRs by explicitly accounting for these characteristics. The mathematical formulation is derived from first principles and is computationally implemented in the open-source depletion code ONIX using neutronics solutions from open-source transport code OpenMC. The new model represents the entire primary loop by dividing it into interconnected depletion zones and tracks nuclide transport, irradiation, and removal mechanisms through a system of coupled ordinary differential equations. This approach enables parallel computation and improves performance over traditional sequential depletion methods. Validation of the developed model against Molten Salt Reactor Experiment data shows good agreement for salt-seeking isotopes and those without noble gas precursors, while discrepancies for other nuclides suggest underestimation of the corresponding removal rates. The depletion model was further applied to a reference Molten Salt Fast Reactor design to assess a new reprocessing scheme intended to expedite the achievement of equilibrium operation.

Keywords: Molten Salt Reactors; circulating fuel system; depletion calculation; burnup analysis; ONIX; OpenMC

1. Introduction

Molten Salt Reactors (MSRs) were first developed in the 1950s and 1960s as part of the Oak Ridge National Laboratory's Aircraft Reactor Experiment (ARE) and Molten Salt Reactor Experiment (MSRE), which demonstrated the feasibility of liquid-fueled reactors [1]. MSRs offer several advantages over conventional solid-fueled reactors, including inherent safety features, online refueling, improved fuel utilization, and the ability to operate on thorium fuel cycles [2]. Their unique fuel-liquid state allows for continuous removal of fission products, reducing long-lived nuclear waste and enhancing reactor performance. Looking forward, MSRs are promising candidates for next-generation reactors, with ongoing research focusing on improving materials, optimizing fuel cycles, and integrating advanced online processing techniques [3]. With growing interest in sustainable nuclear energy, MSR is poised to play a key role in the future of low-carbon power generation.

In the operation of MSRs, unlike most conventional solid-fueled reactors, the liquid fuel salt is continuously circulated in the primary loop while being irradiated in the core

Academic Editor: Dan Gabriel Cacuci

Received: 28 November 2025
Revised: 11 January 2026
Accepted: 10 February 2026
Published: 18 February 2026

region only [4,5]. Therefore, the fuel salt composition undergoes continuous changes due to depletion of fissile isotopes, production of fission products, transmutation in neutron flux, radioactive decay, deposition on various surfaces, transfer to gaseous bubbles, and corrosion products transport to the liquid phase. Fuel salt can also escape the primary loop in the form of mist through the off-gas system. Moreover, sealing and lubrication materials can leak into the primary loop. Other processes can be considered in the operation of MSRs including addition of fissile isotopes, and continuous removal of fission products by mechanical and/or chemical processes. As a result, the isotopic evolution of the fuel salt depends not only on in-core fuel burnup phenomena but also on flow-related processes such as mixing, transport delays, and deposition on system surfaces. Unlike solid-fueled reactors, where fuel composition changes occur locally within fixed assemblies, MSR fuel is continuously circulated, leading to a more dynamic and spatially distributed evolution of isotopes.

Owing to the unique fuel evolution characteristics of MSRs, the point depletion model [6,7], although effective for solid-fueled reactors, is insufficient to capture the diverse physical and chemical phenomena governing MSR fuel behavior. In conventional reactors, depletion models assume isotopes remain in a fixed location, permitting spatially independent burnup calculations. In MSRs, however, isotopes circulate through multiple regions of the reactor, experience varying neutron flux conditions, and undergo selective removal or redistribution. As a result, accurately modeling fuel depletion under circulating conditions requires tracking species transport throughout the entire primary loop and accounting for factors such as fuel residence time, flow patterns, and the selective extraction of fission products. This level of detail substantially increases the complexity of depletion simulations. Even in a one-dimensional model, the computational cost remains high because a large number of isotopes must be tracked over long operational time scales. The resulting number of degrees of freedom renders fully spatially resolved depletion calculations computationally intractable.

On the other hand, the evolution of fuel composition in MSRs remains an active area of research, as the continuous circulation of liquid fuel introduces challenges that are not present in conventional solid-fueled reactors. To address these challenges, multiple computational tools have been enhanced to simulate depletion of fuel-circulating systems, incorporating mechanisms for continuous isotope addition and removal. One such effort is an extended version of the Serpent-2 code, which has been enhanced to simulate circulating fuel behavior [8]. This model applies a point depletion approach, incorporating a decay-like effective removal time constant to account for the extraction of fission products. A similar approach has been implemented into the SCALE code suite, where isotopes can be tracked across multiple material streams, enabling a more flexible treatment of fuel circulation effects [9]. An alternative method has been implemented in the Advanced Dimensional Depletion for Engineering of Reactors (ADDER) software [10], which models the circulating-fuel system as a sequence of discrete components representing different sections of the loop, such as the core, heat exchanger, and external processing units. This approach offers a more physically accurate representation of fuel depletion compared to the uniform composition assumption. However, one drawback of this method is its computational intensity, as calculations must be performed for every instance in which the fuel salt moves through a component within a single depletion time step. Additionally, this approach lacks computational parallelization, since each calculation relies on the outcome of the previous step, restricting efficiency improvements through parallel computing [10].

The objective of this work is to develop an efficient and accurate method for depletion calculations in circulating fuel systems that accounts for the fuel circulation between irradiated and unirradiated zones as well as the relevant chemical and physical removal

mechanisms. The developed approach aims to reduce computational cost by enabling parallelization of the solver and eliminating the need for successive evaluations of fuel compositions in each component. This is achieved through the derivation of a multi-point depletion model from first principles (e.g., mass balance). The central idea is to treat the system components as a network of connected depletion cells. This enables the use of the flow continuity equation to model material transfer between cells and the mass balance equation to describe changes in isotopic densities resulting from this flow. In this formulation, each isotope in each depletion cell is treated as a dependent variable. Then a system of ordinary differential equations (ODEs) can be formed to incorporate all processes that affect the density of all tracked isotopes. This enables the use of existing tools from the linear algebra toolkit to efficiently solve them for the evolution of salt composition along with the inventory in various holdup tanks and surfaces. The developed model is highly versatile and can be applied to a range of nuclear engineering challenges, including fuel management, chemistry control, activation analysis, and radioactivity calculations. Its ability to accurately track isotopic inventories in various holdup tanks and reactor surfaces makes it a suitable approach for modeling and optimizing MSR fuel cycle analysis.

Although the multi-point depletion model can, in principle, be adopted by many burnup modules, in this work it is implemented here within the framework of the generic depletion code ONIX [11], an open-source tool dedicated for fuel depletion modeling in nuclear reactors. ONIX is designed to be flexible and user-friendly, leveraging Python3-based interfaces to facilitate integration with other nuclear engineering tools. It employs point depletion equations and supports various solvers capable of efficiently handling stiff systems of differential equations. A notable feature of ONIX is its ability to couple with the open-source neutron transport code OpenMC [12], enabling fully self-consistent depletion calculations. Its modular structure design also facilitates adaptation to a wide range of reactor concepts, making ONIX a valuable research tool. The multi-point depletion model, together with the example cases described in this paper, is publicly accessible via a GitHub repository [13].

Several recent studies on MSR depletion modeling came to our attention during the preparation of this paper. Fei et al. [14] demonstrated Griffin's MSR depletion capability using the MSRE operational history and performed parametric studies on removal rates, providing valuable early validation despite the current implementation's reliance on constant-flux depletion and fixed one-group cross sections. Seifert et al. [15] introduced a one-dimensional advection-based depletion model, although the method still relies on simplified one-group neutronics and limited thermal–hydraulic coupling. Zhang et al. [16] developed MACT, a versatile depletion code for MSR burnup analysis that integrates external feed model and multi-node nuclide migration effect, demonstrating strong numerical accuracy despite relying on one-group cross sections and simplified migration physics. Although MACT employs techniques similar to certain aspects of our workflow, our method was conceived and implemented independently, prior to the publication of that work. In addition, the present study includes rigorous model validation using the MSRE data. The intended role of the present code is to provide mid-fidelity depletion calculations suitable for scoping and exploratory analyses, and it has been applied to molten salt reactor safeguards studies [17], with ongoing use for estimating proliferation resistance attributes and waste generation metrics.

The remainder of this paper is organized as follows. Section 2 presents the theory and detailed derivation of the multi-point depletion model. Section 3 describes the computational implementation of the MSR depletion module in ONIX. Section 4 introduces the depletion benchmark based on MSRE data and the corresponding validation activities.

Section 5 applies the model to a reference Molten Salt Fast Reactor design. Finally, Section 6 provides concluding remarks and future research directions.

2. Theory and Methodology

The evolution of material composition in *stationary* fuel reactors is governed by production and transmutation in neutron flux field and the decay of radioactive isotopes. The rate of change in the number of atoms for a given isotope can be modeled by the Bateman equation [18] given as

$$\frac{dn_i^{cell}}{dt} = \underbrace{\sum_{j:fissionable} y_{j\to i} \int_{V^{cell}} dV \int dE \sigma_{f,j}(E) n_j^{cell} \phi(t,r,E)}_{\text{Production by fission yield}} - \underbrace{\int_{V^{cell}} dV \int dE \sum_j \sigma_{i\to j}(E) n_i^{cell} \phi(t,r,E)}_{\text{Loss by transmutation to other isotopes}} + \underbrace{\sum_{j\neq i} \int_{V^{cell}} dV \int dE \sigma_{j\to i}(E) n_j^{cell} \phi(r,E)}_{\text{Production by transmutation of other isotopes}} - \underbrace{\lambda_i n_i^{cell}}_{decay} + \underbrace{\sum_{j\neq i} b_{j\to i} \lambda_j n_j^{cell}}_{\text{Production by decay of other isotopes}}, \quad (1)$$

where n_i^{cell} is the number of the i^{th} isotope atoms within a given cell in the geometry, V^{cell} is the cell volume, $y_{j\to i}$ is the fission yield of the i^{th} isotope from the j^{th} fissionable isotope, $b_{j\to i}$ is the branching ratio of the decay of the j^{th} isotope into the i^{th} isotope, σ represents the energy condensed (i.e., one-group) microscopic cross section while $\sigma_{j\to i}$ indicates the *transmutation* cross section from the j^{th} isotope to the i^{th} isotope, and the remaining symbols have standard definitions in nuclear engineering literature. Note that the physical meaning of each term appearing on the right-hand-side of Equation (1) is briefly described using underlined annotations in the equation.

In practice, Equation (1) is solved for the nuclide density (i.e., isotopic concentration) of a given isotope that is defined by

$$N_i^{cell} = \frac{n_i^{cell}}{V^{cell}}. \quad (2)$$

Thus, the nuclide density equation can be readily obtained by dividing Equation (1) by cell volume. When considering the full set of isotopes used in reactor physics applications, a linear system of ODEs can be formed to track all isotopic compositions in the cell. The system may be expressed in matrix form as

$$\frac{d\mathbf{N}^{cell}}{dt} = \left(\varphi^{cell}\boldsymbol{\Sigma} + \mathbf{D}\right)\mathbf{N}^{cell}, \quad (3)$$

where $\mathbf{N}^{cell} = \begin{bmatrix} N_1^{cell} & N_2^{cell} & \cdots & N_m^{cell} \end{bmatrix}^T$ and m represents the total number of isotopes under consideration, and the depletion matrix

$$\varphi^{cell}\boldsymbol{\Sigma} + \mathbf{D} = \begin{bmatrix} -\varphi^{cell}\sum_j \sigma_{1\to j} - \lambda_1 & \varphi^{cell}(\sigma_{2\to 1} + y_{2\to 1}\sigma_{f,2}) + b_{2\to 1}\lambda_2 & \cdots & \varphi^{cell}(\sigma_{m\to 1} + y_{m\to 1}\sigma_{f,m}) + b_{m\to 1}\lambda_m \\ \varphi^{cell}(\sigma_{1\to 2} + y_{1\to 2}\sigma_{f,1}) + b_{1\to 2}\lambda_1 & -\varphi^{cell}\sum_j \sigma_{2\to j} - \lambda_2 & \cdots & \varphi^{cell}(\sigma_{m\to 2} + y_{m\to 2}\sigma_{f,1}) + b_{m\to 2}\lambda_m \\ \vdots & \vdots & \ddots & \vdots \\ \varphi^{cell}(\sigma_{1\to m} + y_{1\to m}\sigma_{f,1}) + b_{1\to m}\lambda_1 & \varphi^{cell}(\sigma_{2\to m} + y_{2\to m}\sigma_{f,2}) + b_{2\to m}\lambda_2 & \cdots & -\varphi^{cell}\sum_j \sigma_{m\to j} - \lambda_m \end{bmatrix}.$$

Here $\varphi^{cell}(t)$ denotes the space-averaged flux at time t given by

$$\varphi^{cell}(t) = \frac{1}{V^{cell}} \int\limits_{V^{cell}} dV \int dE \phi(t, r, E). \tag{4}$$

The isotopic composition for any cell (i.e., depletion zone) can be tracked by solving Equation (3). For *stationary* fuel reactors, the cells are assumed to be isolated, with no mass transfer across the cell boundaries. This permits solving a set of independent instances of Equation (3), each representing an individual cell in the system.

Considering a fuel-circulating loop operating at a volumetric flow rate Q, the number of isotopes transported from cell k to its downstream cell l can be estimated as $f_{k\to l} Q \mathbf{N}^k$, where $f_{k\to l}$ denotes the fraction of the flow that moves from cell k to cell l. As a result of this transport effect, the concentration in cell k is reduced by $f_{k\to l} Q \mathbf{N}^k / V^k$, and the concentration in cell l is increased by $f_{k\to l} Q \mathbf{N}^k / V^l$. To account this spatial transport effect in the depletion calculation, the balance equation of isotopes in the cell k can be extended from Equation (3) and expressed as

$$\frac{d\mathbf{N}^k}{dt} = \left(\varphi^k \mathbf{\Sigma}^k + \mathbf{D}^k\right)\mathbf{N}^k - \sum_{l:downstream} \frac{f_{k\to l} Q}{V^k} \mathbf{N}^k + \sum_{l:upstream} \frac{f_{l\to k} Q}{V^k} \mathbf{N}^l, \tag{5}$$

where the first two terms on the right-hand-side retain the same contribution as in Equation (3), while the third term counts for the rate of change in concentration due flow to the downstream cells, and the last term counts for the rate of change in concentration due to flow from the upstream cells.

In the new formulation of the depletion model for circulating-fuel systems, the composition of connected cells is coupled. Therefore, the isotopic compositions in all cells of the entire fuel loop can be expressed in a matrix form as

$$\frac{d\mathbf{N}^{sys}}{dt} = \mathbf{R}\mathbf{N}^{sys}, \tag{6}$$

where $\mathbf{N}^{sys}$ is a stacked vector of all cells' compositions (size $m \times n$) with n stands for the total number of cells, and the *extended* depletion matrix

$$\mathbf{R} = \begin{bmatrix} \varphi^1 \mathbf{\Sigma}^1 + \mathbf{D}^1 - \frac{Q}{V^1}\mathbf{F}_{1\to} & \frac{Q}{V^1}\mathbf{F}_{2\to 1} & \cdots & \frac{Q}{V^1}\mathbf{F}_{n\to 1} \\ \frac{Q}{V^2}\mathbf{F}_{1\to 2} & \varphi^2 \mathbf{\Sigma}^2 + \mathbf{D}^2 - \frac{Q}{V^2}\mathbf{F}_{2\to} & \cdots & \frac{Q}{V^2}\mathbf{F}_{n\to 2} \\ \vdots & \vdots & \ddots & \vdots \\ \frac{Q}{V^n}\mathbf{F}_{1\to n} & \frac{Q}{V^n}\mathbf{F}_{2\to n} & \cdots & \varphi^n \mathbf{\Sigma}^n + \mathbf{D}^n - \frac{Q}{V^n}\mathbf{F}_{n\to} \end{bmatrix}.$$

Here $\mathbf{F}_{k\to l}$ is a diagonal matrix with its diagonal elements set as $f_{l\to k}$, and $\mathbf{F}_{k\to} = \sum\limits_{l\in upstream} \mathbf{F}_{k\to l}$ represents the total flow leaving the cell k. Each term in the *extended* depletion matrix $\mathbf{R}$ is a square matrix of size $m \times m$.

Equation (6) presents a new multi-point depletion model that effectively describes the evolution of all cells' compositions in a flow field. The model employs a finite-volume framework to represent depletion cells and applies continuity equations to capture mass flow between them. The resulting changes in isotopic concentration from the circulating flow are incorporated directly into the Bateman equation for burnup calculations, which removes the need for advection-based mass transport models and avoids the numerical instabilities associated with coarse spatial discretization. Note that the fuel flow can also give rise to additional phenomena, such as noble metal deposition, noble gas volatilization, and other engineered processes in MSRs, including online refueling and reprocessing. To account for these effects, Equation (6) can be readily modified by incorporating the

corresponding addition or removal rates into the appropriate terms on the right-hand-side of the equation.

The total number of dependent variables in Equation (6) is $m \times n$, representing all the tracked isotopes in all depletion cells, but all reactions considered in Equation (6) depend only on the isotopic compositions existed in the system. Hence, the balance equation is governed by a homogeneous system that can be readily solved by the Chebyshev rational approximation method, or short as CRAM [19]. However, in some other scenarios, such as online refueling or reprocessing, these source terms cannot be expressed in terms of the system state. In this case, Equation (6) can be extended by adding an external source term

$$\frac{d\mathbf{N}^{sys}}{dt} = \mathbf{R}\mathbf{N}^{sys} + \mathbf{S}, \tag{7}$$

where $\mathbf{S}$ is a vector of length $m \times n$ (in units of $\mathrm{cm}^{-3}\cdot\mathrm{s}^{-1}$) representing the external source term. The general solution of Equation (7) can be expressed as the sum of a homogeneous component and a particular component. For a given time step Δt, the general solution takes the form of

$$\mathbf{N}^{sys}(t+\Delta t) = e^{\mathbf{R}\Delta t}\mathbf{N}^{sys}(t) + \int_{t}^{t+\Delta t} e^{\mathbf{R}(t+\Delta t-\tau)}\mathbf{S}d\tau. \tag{8}$$

Here the first term on the right-hand-side of the equation is known as the homogeneous component that can be obtained from Equation (6) using the CRAM, and the second term is the particular component that can be obtained using the property of the matrix exponential and its integral

$$\int_{t}^{t+\Delta t} e^{\mathbf{R}(t+\Delta t-\tau)}\mathbf{S}d\tau = \mathbf{R}^{-1}\left(e^{\mathbf{R}\Delta t} - \mathbf{I}\right)\mathbf{S}, \tag{9}$$

where $\mathbf{I}$ is the identity matrix. Equation (9) can be further expressed in the form of

$$\mathbf{R}^{-1}\left(e^{\mathbf{R}\Delta t} - \mathbf{I}\right)\mathbf{S} = \mathbf{R}^{-1}\left[e^{\mathbf{R}\Delta t}\mathbf{S} - \mathbf{S}\right]. \tag{10}$$

This provides more convenience to compute the operation of the exponential matrix on the external source vector using the CRAM.

In the derivation of the depletion model for the circulating-fuel system, it was assumed that each cell is filled with a homogenous material (i.e., each cell is considered as a perfect mixing pot). The validity of this assumption increases as the cell size decreases. However, even with larger cell volumes, the fuel residence time in the cell estimated by Q/V^{cell} is sufficiently small compared to the time scale for other phenomena such as isotope transmutation and decay, which means the salt mixing process is much faster than other processes that affect the concentration and validates the homogenous composition assumption.

The multi-point depletion model given in Equation (7) can be efficiently solved as a fully coupled system using advanced linear algebra techniques. All depletion cells are assembled into a single system matrix, which provides a mid-fidelity capability for MSR burnup analysis. The size of the depletion matrix equals the square of the number of degrees of freedom $(m \times n)^2$. Since the runtime for the CRAM is known to grow with the cube of the system matrix size, the CRAM solution time is then proportional to $(m \times n)^3$. This represents a limiting boundary on the number of cells and/or the number of isotopes to be tracked. However, the runtime spent by the CRAM solver is typically negligible compared to that of the transport solver, especially when the Monte Carlo transport method is used. To put this into perspective, for the MSRE benchmark problem discussed in Section 4, using two depletion cells and tracking 1637 isotopes on a single core, each CRAM execution

added only 15 s to the runtime, compared with approximately 25 min for each OpenMC transport calculation. Increasing the number of cells from two to three raised CRAM runtime to 75 s. For the four-cell case results as presented in Section 4, the CRAM runtime increased to 175 s. The runtime of the particular solution typically takes a few seconds more than the homogenous solution due to the time required for additional operations like inverting the depletion matrix, but overall the CRAM runtime is insignificant relative to that of the transport calculation.

One additional note on the discretization of the circulating fuel system into multiple depletion cells is that it plays an important role in capturing spatial variations in flux, cross sections, and local removal phenomena. Increasing the number of cells improves solution accuracy in two primary ways: by providing higher spatial resolution for cell-averaged neutron flux and reaction rates, and by enabling more detailed representation of localized material transport and depletion effects. However, for MSR systems, the neutron flux is expected to be relatively uniform due to the absence of solid fuel heterogeneities, and the short fuel circulation times promote strong homogenization of isotopic inventories throughout the loop. As a result, key integral quantities such as the effective multiplication factor and isotope inventories are expected to exhibit rapid convergence with respect to the number of depletion cells. Beyond a moderate spatial resolution, further refinement is therefore anticipated to yield diminishing returns relative to the associated increase in computational cost. This behavior is consistent with prior MSR analyses and supports the robustness of the proposed multi-point depletion approach.

3. Computational Implementation

In this work, the multi-point depletion model for MSRs is implemented in the open-source depletion software ONIX, which is primarily written in the object-oriented Python language but can be integrated with C++ libraries or other codes written in different languages. During the implementation, a new module named *'msr'* is developed within the ONIX framework. The class *'Couple_msr'* inherited the existing class '*Couple_openmc*', which establishes a coupling link between the depletion calculation in ONIX and the neutron transport simulation in OpenMC. Through the new module, the user can define the depletion cells, the configuration of the fuel circulation loop, the salt flow rate, and the rates of special addition or removal of isotopes.

The burnup calculation starts with the specifications of the OpenMC model. All depletion cells must be defined as physical cells in OpenMC including unirradiated cells (i.e., cells with zero neutron flux). Once the OpenMC model is established, the user can create an instance of the *'Couple_msr'* class, which takes a depletion dictionary named '*loop_dict*' as input to define the depletion cells. Table 1 describes the entries in the depletion dictionary that is used in the MSR module. The module also allows the user to define the list of isotopes to be tracked in each depletion cell during the burnup calculation. At present, all cells share the same isotope list.

Once the reactor configuration is specified, the code constructs a connectivity matrix that defines the rate of change of all dependent variables resulting from flow-related phenomena and other designed processes. The user initializes the burnup analysis by specifying the power and defining the burnup sequence according to macro-depletion steps (macro-steps). At the start of each macro-step, OpenMC performs the eigen-mode transport calculation and generates the energy condensed cross section (i.e., One-group cross sections) and the spatial averaged flux for each cell. The ENDF/BVIII.0 cross section library [20] was used in OpenMC calculations. The cell-averaged flux is then scaled based on the power or flux normalization condition. The cross section and scaled flux are then passed to the ONIX module to perform the depletion calculation for that macro-step. In

the current implementation, the coupling between neutron transport and depletion is one-way, with no predictor–corrector or iterative strategy employed within a depletion step. The drift effect of delayed neutron precursors is not explicitly modeled in the present work. Although the multi-point depletion formulation tracks the flow and transmutation of all nuclides that physically constitute delayed neutron precursors, the treatment of delayed neutrons in OpenMC relies on a fixed set of artificial precursor groups whose properties are independent of the cell-wise isotopic composition provided by the depletion solver. As a result, the Monte Carlo transport calculation effectively assumes a stationary precursor distribution within each transport snapshot. This limitation arises from the structure of the delayed neutron data and their implementation in current Monte Carlo transport codes rather than from the proposed depletion formulation, and it implies that kinetics-related parameters influenced by precursor drift are treated as quasi-static at the snapshot execution time.

Table 1. The '*loop_dict*' dictionary used to define depletion cells in the MSR modular.

Variable	Description
Dictionary key	A string representing the name of an OpenMC cell
'upstream_cells'	A list of tuples in which the first item is the name of one upstream cell relative to the current cell, and the second item is the fraction of the flow rate coming from that cell.
'elements_removal'	A list of tuples in which the first item is the name of one element that is being removed from the current cell, and the second item is the removal rate defined as the fraction of atoms removed per second.
'nuclide_removal'	Similar to the 'elements_removal' but used to specify individual isotopes rather than all isotopes of an element. For example, the string 'U-235' can be used to identify that specific isotope.
'external_nuclide_addition'	Similar to the 'nuclide_removal', the addition rate is defined as the number of external atoms added per second. Thus, it is treated as a fixed external source.
'holdup'	Used for cells that do not receive a flow of salt but instead receive specific elements, such as an off-gas system or a deposition surface. This key accepts a list of tuples in which the first item is the name of the feed cell, and the second item is a list of tuples similar to those used in 'elements_removal'.
'external_salt_stream'	Used to define an external feed stream of salt with a known composition. It accepts a tuple in which the first item is the flow rate of the feed stream and the second item is a list of tuples, each containing one isotope and its density in the feed stream (in units of $barn^{-1} \cdot cm^{-1}$). The algorithm automatically removes an equal flow rate from the cell to conserve the total salt volume.
'recycling'	Used to define the recycling of selected isotopes to another cell—such as recycling U-233 from the blanket to the core. It accepts a tuple in which the first item is the name of the destination cell, and the second item is a list of tuples, each containing one element and its recycling rate as a fraction of the cell concentration per second. Note: the user must still specify the removal of these elements from the original cell using 'elements_removal'.

Each macro-step is typically subdivided into a user-specified number of micro-depletion steps (micro-steps) in order to solve the depletion equation given in Equation (7).

For each micro-step, the 16th-order CRAM solver [19] built in ONIX is employed to compute the homogenous component of the solution given in Equation (8). If the external source is non-zero, the particular component of the solution is computed using Equation (10) by leveraging the CRAM solver. The computation involves inverting the depletion matrix. The robust NumPy solve function [21] is used to solve the system matrix to avoid inverting a singular matrix. At the end of each micro-step, the particular solution is added to the homogenous solution to obtain the final isotopic density at this time step. At the end of each macro-step, the material composition calculated by the ONIX module is passed back to the OpenMC model, which updates the material composition and performs transport calculation for the subsequent macro-step. This process is repeated until the end of the user-specified macro-step is reached. Figure 1 provides a brief overview of the computational flow between the ONIX and OpenMC modules in the depletion calculation.

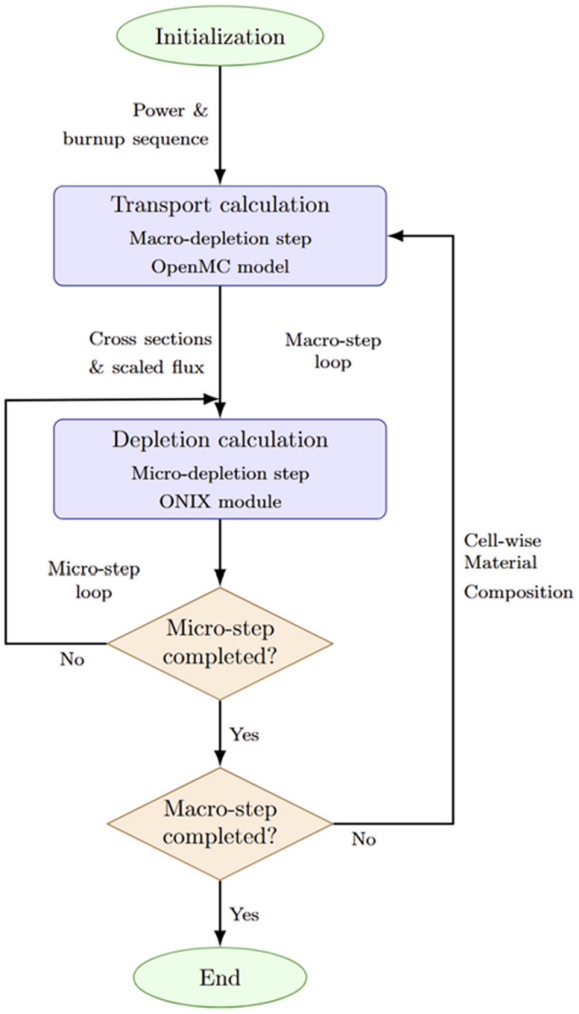

Figure 1. Flowchart of the MSR depletion modules implemented in ONIX.

4. Model Validation with MSRE Data

The Molten Salt Reactor Experiment (MSRE) was a thermal spectrum MSR operated between June 1965 and December 1969 and served in demonstrating the circulating-fuel concept. The FliBe salt mixture (LiF-BeF_2) was used as a fuel carrier in the primary loop in MSRE. The reactor was initially fueled with uranium with 33 wt.% U-235 enrichment. In the second phase, which started in August 1968, uranium with 91 wt.% U-233 enrichment was added to the fuel salt after removing the remaining uranium charge from the first phase. MSRE was moderated by a graphite matrix, and all structural components and piping are

constructed of Hastelloy N, a nickel-based alloy containing about 17% molybdenum, 7% chromium, and 5% iron. The total fuel salt volume in the primary loop was about 1.958 m^3, of those 1.618 m^3 filled the reactor vessel. At nominal operation flow rate (1200 gpm), 5% of the flow (65 gpm) was recirculated in the pump bowl which had a fluid capacity of 0.136 m^3 and operated about 60% full. The pump bowl was equipped with an off-gas system to remove as much xenon and krypton fission gases as possible. Purified helium was used as purge gas, entering the pump bowl gas space at a normal rate of 3.29 std liters/min. The best estimate of the MSRE maximum power is 7.34 $\pm$ 0.09 MW [22]. The MSRE design and operation conditions are discussed in detail in Refs. [23–26].

During the MSRE program, experimental data were collected from various sources to indicate the fission product behavior in the MSR system including samples in the form of capsules of liquid or gas taken from the pump bowl periodically, surveillance specimens of material recovered from various system segments, as well as surveys of gamma radiation using remote collimated instrumentation [27]. For systematic studies, fission products are generally categorized into four groups based on their chemical behavior. The first category consists of stable salt-soluble fluorides that include the lanthanides, yttrium, zirconium, rubidium, cesium, silicon, and barium. All of these elements form stable fluorides that are soluble in fuel salt. These fluorides would thereby be expected to be found completely in the fuel salt except in those cases where there is a noble-gas precursor of sufficiently long half-life to be appreciably stripped to off-gas. The second category consists of the noble metals that include niobium, molybdenum, technetium, ruthenium, silver, antimony, and tellurium. Noble metals form a particulate pool that is circulated with salt and can be deposited on various surfaces or carried out in the purge gas to the off-gas system. The analysis of gas samples during the U-235 operation showed that 30 to 100% of the noble metals being produced in the MSRE fuel system were transported to the off-gas system. The third category consists of the noble gases that essentially include krypton and xenon. Noble gases are removed from the fuel salt by stripping to the off-gas during the bypass flow through the pump bowl. The fourth category includes tellurium and iodine that largely remain in the salt with no evidence of volatilization or deposition on metal or graphite surfaces [27].

In this study, the primary experimental data used for the depletion model validation is the activity of salt samples taken from the MSRE pump bowl during the U-235 phase operation. The data is organized in detail into four categories described above in Table 6.7 of Ref. [27]. The original data are reported in units of curies per gram of the sample. For benchmarking purposes, these data were converted to units of atom/cm^3 by multiplying the salt density and dividing the decay constant of each isotope. The salt density was taken to be 2.3243 g/cm^3 in the process. The unit-converted experimental data is presented in Section 4.2 for comparison with simulation results.

4.1. Benchmark Specifications

To effectively use the measurements of the concentration of fission products in the MSRE salt, the operation history of the reactor during the U-235 phase needs to be quantified. The power operation of the MSRE started with run 4 on 23 January 1966. The U-235 phase ended with run 14 on 25 March 1968. The power history of the MSRE is recorded in graphical format in Figure 3.1 of Ref. [27]. The power history was digitalized and provided in tabular form in Ref. [28]. In the process of digitalizing the power history, the authors assumed that the full power corresponded to 7.34 MW and converted periods of ramp power into a period with time-averaged constant power. The power history provided in Ref. [28] is shown graphically in Figure 2 and used in the benchmark model.

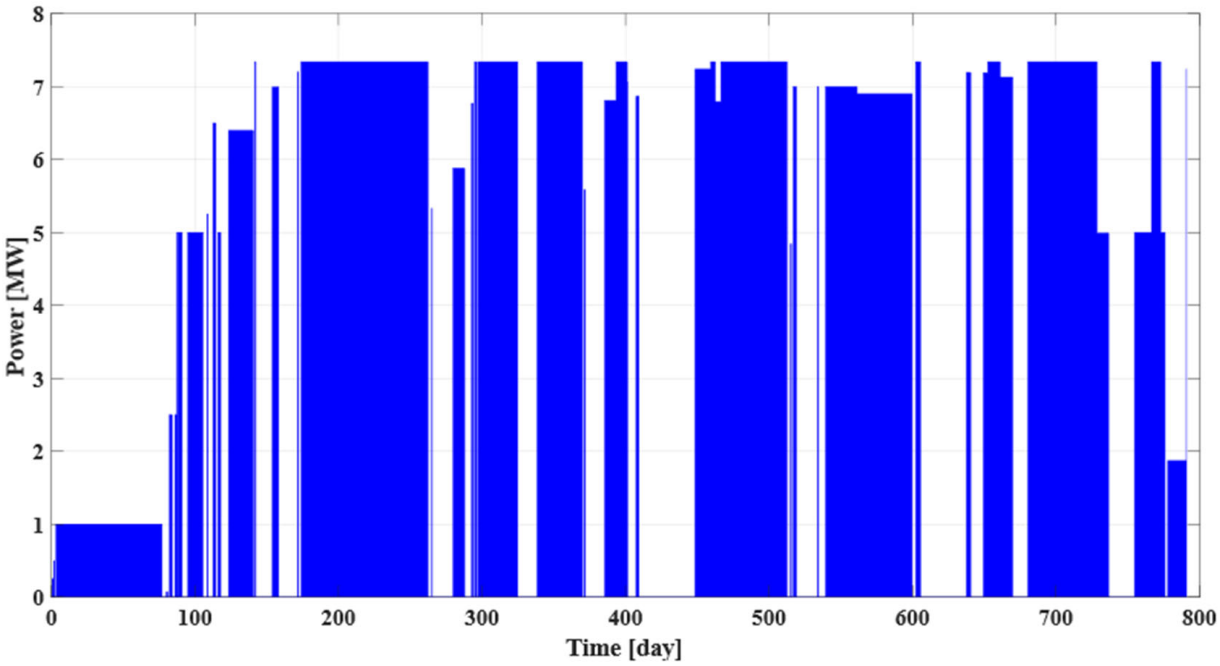

Figure 2. The power history of the MSRE between the start of run 4 and the end of run 14. (Source: Table 2-2 of Ref. [28]).

A simplified geometry of the MSRE vessel is used for neutronics calculation. The geometry of the upper and lower heads is simplified using right cylinders conserving the total volume. The control rod channels are filled with fuel salt, and the top tapered surfaces of graphite stringers are removed. Finally, the fuel inlet, flow distributor, internal structures, and fuel outlet are ignored. The external loop and pump bowl are added on top of the reactor vessel as right cylinders. This placing of external components does not affect the neutronics simulation as it is located outside the vacuum boundary condition. The volumes of the depletion cells are 1.2885 m^3, 0.6174 m^3, and 0.0816 m^3 for the core, loop, and pump bowl cells, respectively. The geometry of the MSRE benchmark model established in OpenMC is shown in Figure 3. The geometrical parameters of the benchmark model are listed in Table 2. All materials are assumed to be at 900 K. The graphite density is 1.86 g/cm^3, and the initial fuel salt density is 2.3243 g/cm^3. The initial composition of the fuel salt is given in Table 3.

Table 2. Dimensions of the MSRE benchmark model.

Parameter	Value [cm]
Size of unit cell	5.08 × 5.08
Fuel channel (width, length, radius)	(1.016, 3.048, 0.508)
Core height	170.18
Upper head height	50.0
Lower head height	50.0
Reactor vessel radius	70. 485
External loop height	45.336
Pump bowl height	5.228

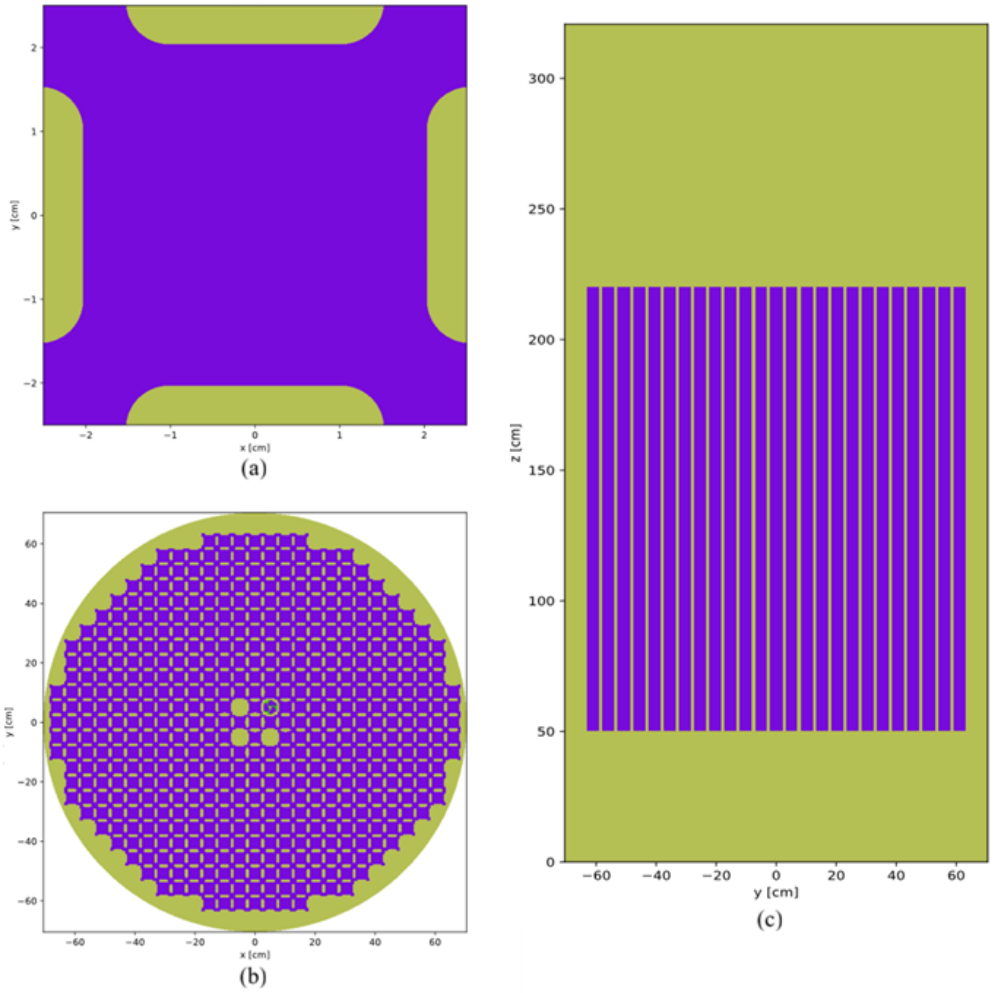

Figure 3. Geometry of the MSRE benchmark model: (**a**) unit cell, (**b**) top view, and (**c**) side view of the reactor. Graphite is shown in purple, and the fuel salt is shown in olive. Note in the central region of the subfigure (**b**), the three green circles represent the control rod tubes, while the fourth, partially shaded circle denotes the sample basket, which provides space for testing materials under irradiation.

Table 3. Initial isotopic composition of the MSRE fuel salt.

Isotope	Atom Fraction
Be-9	1.18×10^{-1}
F-19	5.94×10^{-1}
Li-6	3.07×10^{-5}
Li-7	2.64×10^{-1}
U-235	1.01×10^{-3}
U-238	2.24×10^{-3}
Zr-90	1.04×10^{-2}
Zr-91	2.27×10^{-3}
Zr-92	3.48×10^{-3}
Zr-94	3.52×10^{-3}
Zr-96	5.68×10^{-4}

The noble gases removal rates and the noble metals deposition rates are not provided explicitly in the MSRE legacy document. To facilitate the use of the available experimental data for validation, the reported data for the gas removal system and deposition intensity is used to estimate the removal rates. To calculate the gas removal rate from the pump bowl, it is assumed that noble gases instantaneously migrate to the purge gas bubbles. Under this assumption, the rate of noble gases removal can be calculated as

$$\lambda_{gas} = \frac{Q_{purge\_gas}}{V_{pump\_bowl}} = \frac{3.29}{60 \times 81.6} = 6.72 \times 10^{-4}\ \mathrm{s}^{-1}. \quad (11)$$

For noble metals, two removal mechanisms are considered: transport to the off-gas system and deposition on various surfaces. As mentioned earlier, 30 to 100% of noble metals are transported to the off-gas system. A lower boundary on the removal rate can be estimated by assuming a liquid to gas mass transfer coefficient of 10^{-4}. Then the rate of noble metals removal by the off-gas system can be calculated as

$$\lambda_{metal} \approx 10^{-4} \times \lambda_{gas} \times 65\% = 4.37 \times 10^{-8}\ \mathrm{s}^{-1}. \quad (12)$$

Finally, the deposition rate can be calculated from the deposition intensity on surveillance specimen array. Table 12.2 of Ref. [27] gives the relative deposition intensity, defined as the ratio of deposited concentration to the calculated concentration if the entire inventory was uniformly deposited on all surfaces. For specimens that were exposed for the last four months of MSRE operations, the deposition rate can be roughly estimated as

$$\lambda_{deposition} = \frac{\text{relative deposition intensity}}{\text{exposure time}}. \quad (13)$$

Table 4 summarizes the removal rates of noble metals and noble gases at different depletion cells of the MSRE benchmark model. The removal mechanism applied to each cell is also clarified in the table.

Table 4. Estimated removal rates in [s^{-1}] for noble metals and noble gases for the MSRE.

Depletion Cell (Mechanism)	Nb	Mo	Ru	Te	Tc	Sb	Zr	Xe
Reactor vessel (deposition)	2.07×10^{-8}	3.53×10^{-8}	1.34×10^{-8}	3.49×10^{-8}	-	-	-	-
Loop (deposition)	2.89×10^{-8}	1.25×10^{-7}	2.89×10^{-8}	1.93×10^{-7}	-	-	-	-
Pump bowl (deposition + off-gas)	7.26×10^{-8}	1.69×10^{-7}	7.26×10^{-8}	2.37×10^{-7}	4.37×10^{-8}	4.37×10^{-8}	6.72×10^{-4}	6.72×10^{-4}

Note that the following phenomena identified by the MSRE team are not considered in the present benchmark model:

(1) The salt spray system in the pump bowl could not be turned off. As a result, the generation of bubbles and salt mist was always present. In addition, the effects were not constant because they depended on the salt level, which varied continuously.
(2) Lubricating oil from the pump bearings entered the pump bowl at a rate of 1–3 cm^3 per day.
(3) There were continuously varying flow and blowback of fuel salt between the pump bowl and an overflow tank.

Other events that took place between run 4 and run 14 and were not included in the model are:

(1) During run 9, a total of 761 g of U-235 was added in the form of LiF-UF4 eutectic salt.
(2) During run 12, a total of 1527 g of U-235 was added using the sampler-enricher.
(3) About 8.6 g of beryllium was added in April 1967, and 38 g was added in July 1967.

Lastly, the exact time of examining each sample was not reported, so it was assumed that each experiment measurement corresponds to noon time of the stated date.

4.2. Simulation Results

Four depletion cells are considered for the MSRE burnup analysis, representing the reactor vessel, loop, pump bowl, and the off-gas tank, respectively. The pump bowl cell contains the salt sample for comparison analysis, and the off-gas tank is simply a holdup tank that receives the gas and allows it to decay. Two sets of depletion calculations were conducted on the MSRE benchmark. In the first set, neither removal by the off-gas system nor by deposition was included. In the second set, element removal rates were applied using the rates listed in Table 4. In both sets of calculations, the maximum micro-step was set to 100 h.

The calculated isotope concentrations in the pump bowl salt were compared to the sample concentrations extracted from Table 6.7 of Ref. [27]. The results are organized into the four categories of elements as discussed before and presented in Figures 4–7, respectively. The uncertainty in power history, operational conditions, and sampling times, along with the limited quality of the experimental measurements, makes point-by-point comparison with the experimental data challenging. However, the calculated inventories are qualitatively compared to the observed concentrations in all the figures. Overall, the results demonstrate qualitative agreement with the experimental data.

As shown in Figures 4 and 5, the agreement for the first two categories—isotopes without noble gas precursors and salt-seeking isotopes—is strong. This is expected, since the entire inventory of these isotopes remains within the fuel salt. Consequently, the predicted inventories are identical in both the removal and no-removal scenarios.

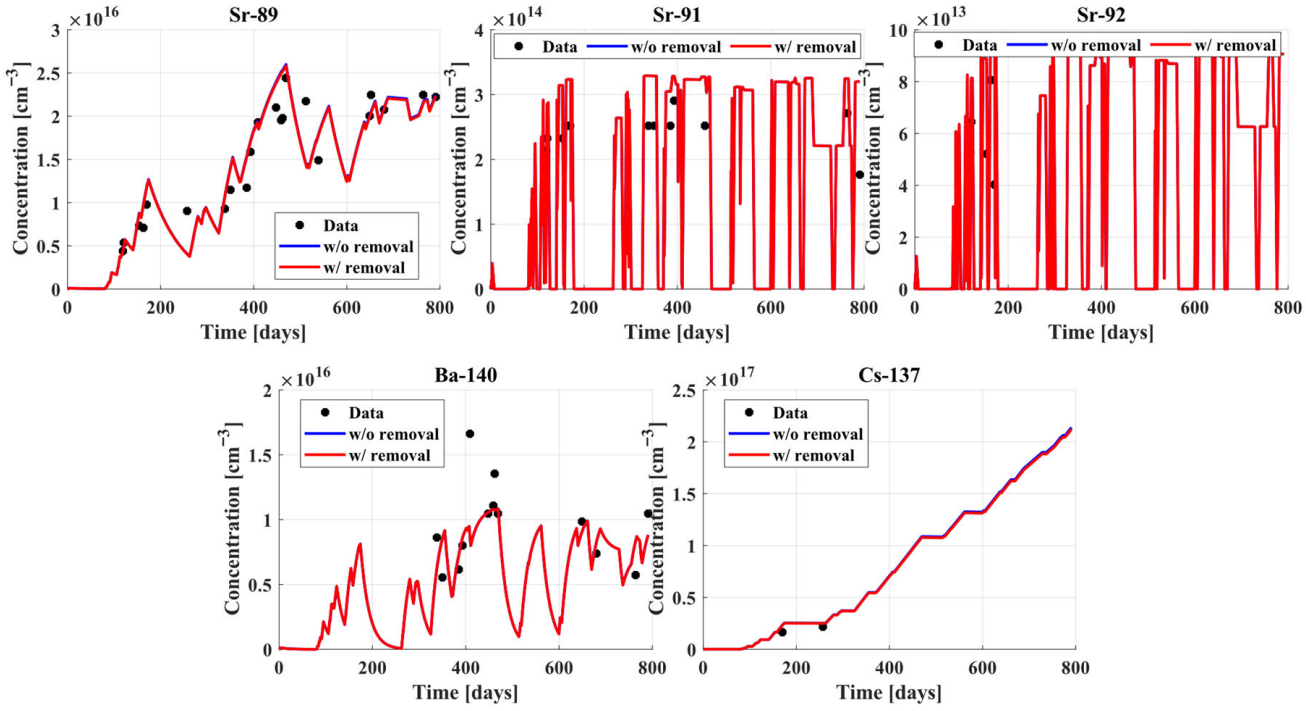

Figure 4. The concentration of isotopes with no noble gas precursors for the MSRE pump bowl.

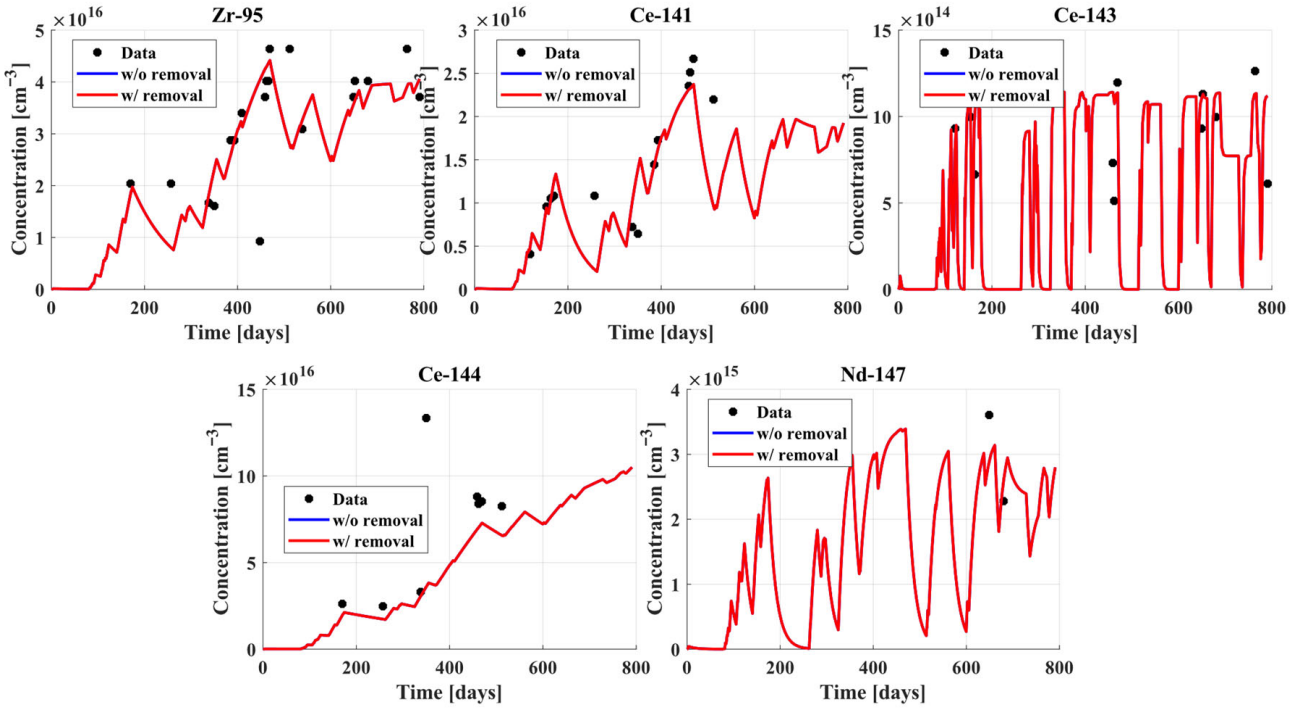

Figure 5. The concentration of salt-seeking isotopes for the MSRE pump bowl.

As shown in Figure 6, the accuracy of the calculated inventories for noble metal isotopes varies by isotope. For Nb-95 (half-life: 35 days), the model overpredicts the inventory in most samples, though a few points align well with the measurements. In contrast, the predictions for Mo-99 (half-life: 66 h) match the experimental data closely. The inventory of Mo-99 is nearly unaffected by removal processes due to its relatively fast decay rate, which is at least an order of magnitude higher than the removal rate. For ruthenium isotopes, the impact of removal is closely tied to half-life. Ru-105 (half-life: 4.4 h) shows negligible sensitivity to removal, while Ru-103 (half-life: 39 h) and Ru-106 (half-life: 372 days) are significantly influenced by it. The calculated inventories for Ru-103 and Ru-106 are noticeably higher than measured values, suggesting that their removal rates may be underestimated. For Ag-111 (half-life: 7.5 days), only a few samples are available. The measured concentrations are reasonably close to the predicted values, though they appear temporally shifted.

As shown in Figure 7, the predictions for iodine isotopes are in fairly good agreement with measurements. However for tellurium isotopes—Te-132 (half-life: 3.2 days) and Te-129m (half-life: 33.6 days)—the calculated inventories are consistently higher than the observed ones, again pointing to a potential underestimation of removal rates. It should be noted, however, that this discrepancy may also reflect limitations in the available experimental data and modeling assumptions beyond the treatment of removal of a limited set of elements. In particular, the legacy MSRE data only reports removal or deposition for a small subset of elements, whereas in reality additional fission products and activation products may have been partially removed or redistributed through chemical interactions, plating, or system holdup. Furthermore, post-operation flushing and subsequent mixing with residual salt introduce dilution effects that are difficult to quantify and are not fully documented. Finally, the conversion of reported relative activities (Ci/g) to absolute isotopic inventories requires assumptions on salt density and decay constants, both of which introduce additional uncertainty. Collectively, these factors complicate the attribution of

discrepancies to any single physical mechanism and limit the degree to which quantitative agreement can be expected from the available dataset.

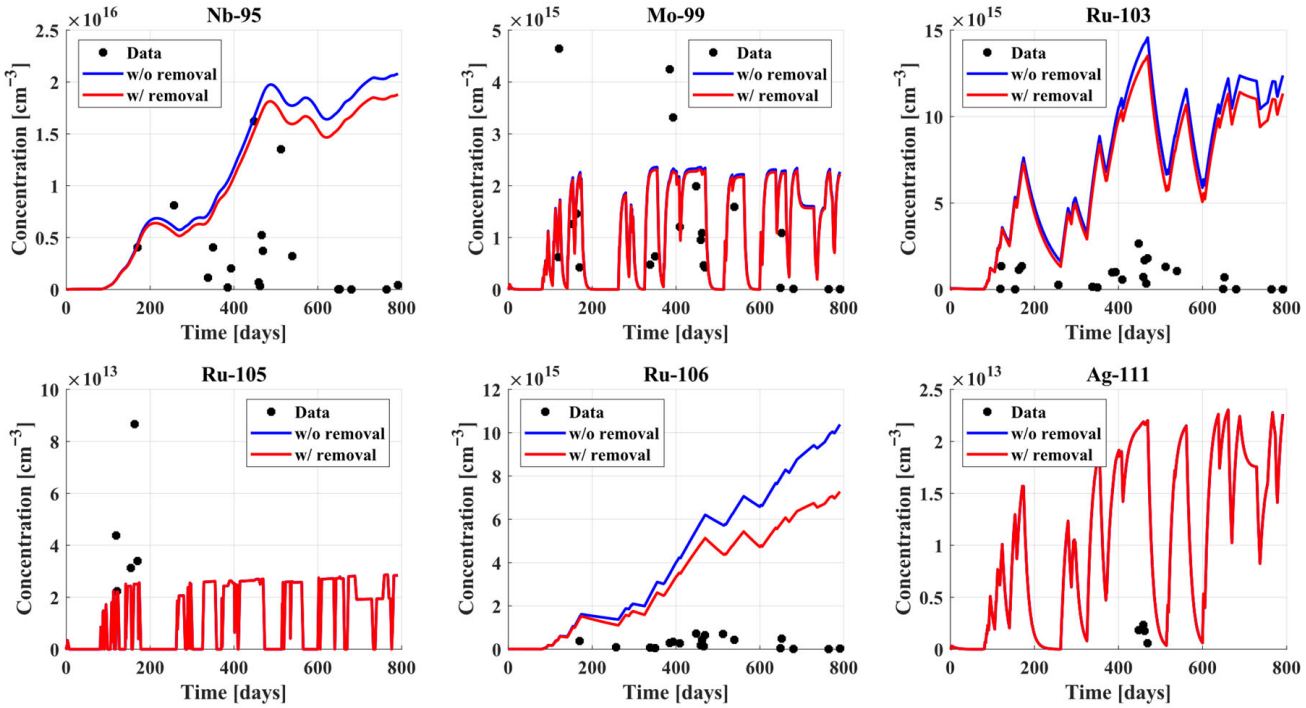

Figure 6. The concentration of the noble metals for the MSRE pump bowl.

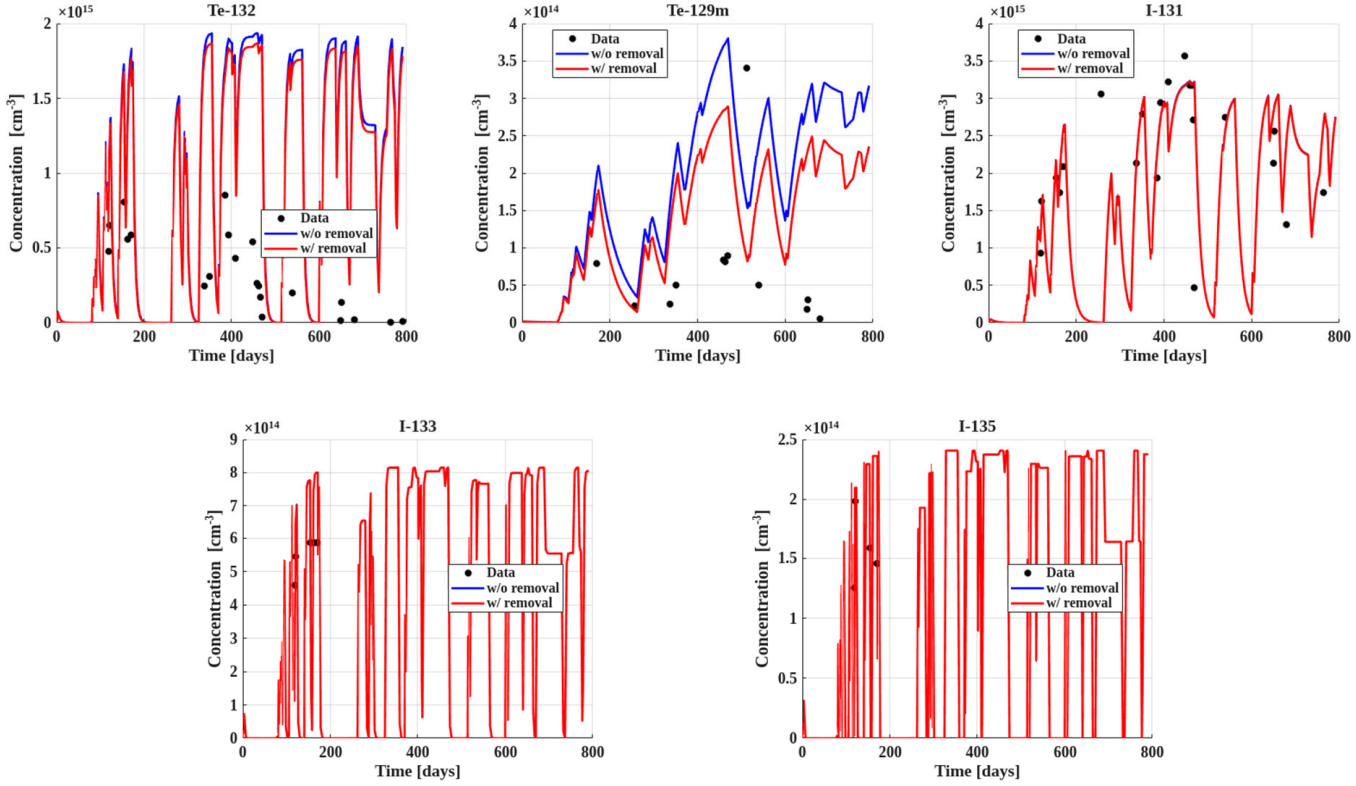

Figure 7. The concentration of tellurium and iodine isotopes for the MSRE pump bowl.

To understand the effect of the off-gas system on the noble gas concentration, Figure 8 shows the concentrations of three gaseous isotopes in the pump bowl in both the removal

and no-removal scenarios. For Kr-85 (half-life 10.7 years), the operation of the off-gas system reduced the concentration by three orders of magnitude. For Xe-135 (half-life: 9.14 h) and Xe-133 (half-life: 5.2 days), the off-gas system reduced the concentration by a factor of two and one order of magnitude respectively.

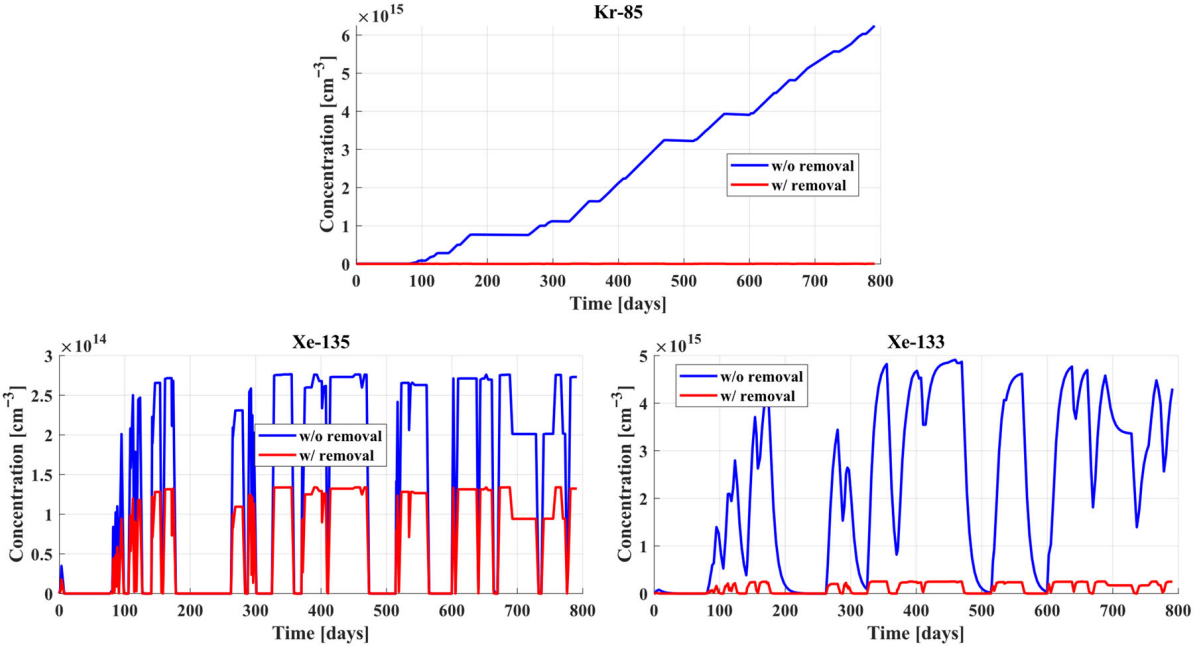

Figure 8. The concentration of some noble gases in the pump bowl for the MSRE.

Finally, Figure 9 shows the effect of isotopes removal on the effective multiplication factor (k_{eff}) of the reactor. As can be seen, the removal of fission products through the off-gas system and surface deposition consistently increased the k_{eff} value by approximately 220 pcm (1 pcm = 10^{-5}).

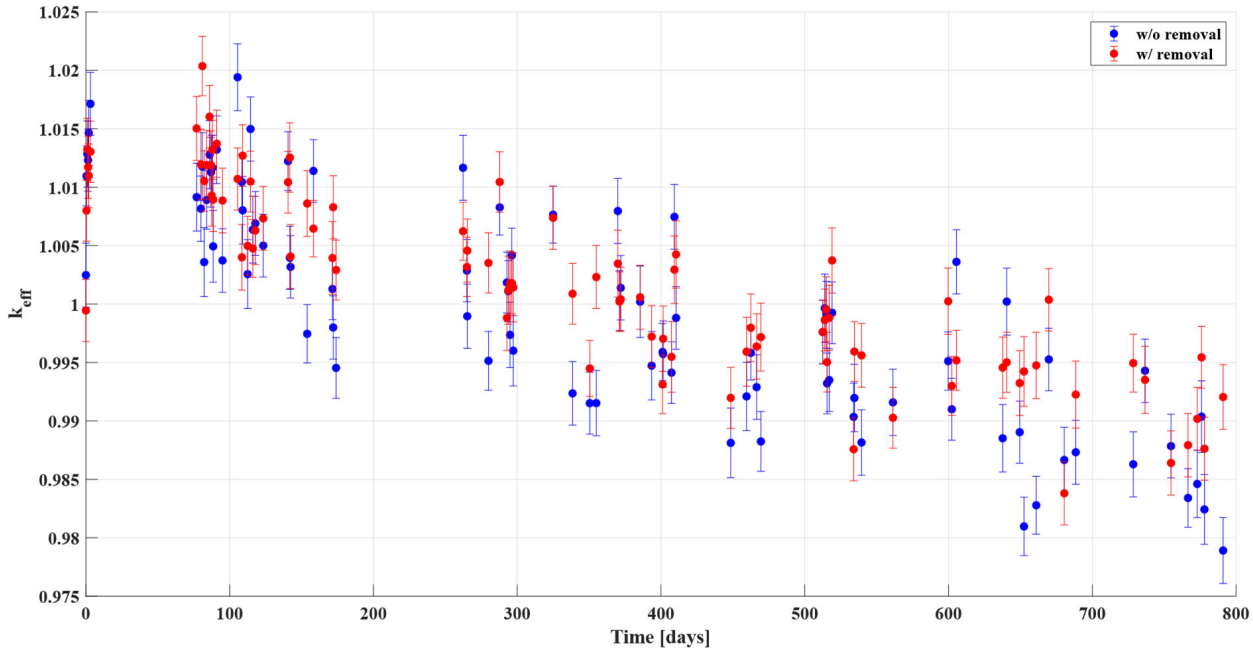

Figure 9. The evolution of k_{eff} during the operation of the MSRE with and without removal scenarios. Error bars represent 1-σ statistical uncertainty from the Monte Carlo calculations.

5. Application to Molten Salt Fast Reactor

The Molten Salt Fast Reactor (MSFR) is a conceptual fast-spectrum MSR that operates in the thorium fuel cycle. MSFR may start either with U-233, U-235 enriched uranium and/or transuranic (TRU) elements. A collaborative effort with participants from the FP7 project EVOL and the ROSATOM project MARS put together a neutronics benchmark for a reference design of MSFR [29]. The participants performed intensive code-to-code verifications to the MSFR benchmark model using various computational tools. In this work, the U-233 started MSFR benchmark model was adopted as an application of the multi-point depletion model.

5.1. MSFR Model Specification

The geometry of the MSFR model consists of a number of concentric cylinders. The entire reactor core is housed inside a cylindrical cavity centered within a larger cylindrical reflector made of nickel-based alloy. The overall cylindrical structure has a diameter of 4.529 m and a height of 4.255 m. The central cavity has a radius of 2.0645 m and a height of 2.255 m. Surrounding the active reactor core, a fertile blanket forms a cylindrical shell with an inner radius of 1.1475 m, an outer radius of 1.6075 m, and a height of 1.840 m. The blanket is encased in a 20 mm thick structural layer made of the same alloy as the reflector. Beyond the blanket, there is a 20 cm thick B_4C neutron protector providing shielding. The rest of the cavity is filled with fuel salt. The overall geometry of the MSFR model established in OpenMC is shown in Figure 10. The density and isotopic composition of the materials in the MSFR model are provided in Table 5. All material properties are estimated at 973.15 K, and the fuel circulation period is ~4 s.

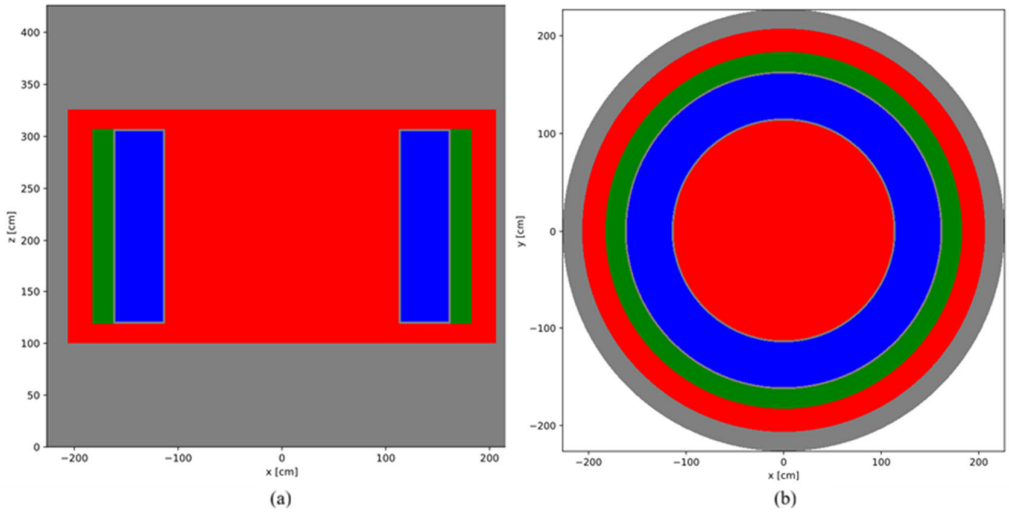

Figure 10. Geometry of the MSFR model: (**a**) side view and (**b**) top view of the reactor. Fuel salt is shown in red, the fertile blanket in blue, B_4C protector in green, and the Ni-based alloy in grey.

An integrated reprocessing plant is required for MSFR to continuous removal of fission products including neutron poisons to maintain an efficient and sustainable chain reaction of the reactor. A number of simplifying assumptions are introduced to model the reprocessing scheme during the MSFR burnup calculation. The gaseous extraction system removes elements from both the fuel salt and the fertile blanket with a removal period assumed to be 30 s. Only the elements with the following atomic numbers are extracted by the system: Z = 1, 2, 7, 8, 10, 18, 36, 41, 42, 43, 44, 45, 46, 47, 51, 52, 54 and 86. An offline reprocessing plant reprocesses the fuel salt at a rate of 40 L per day to remove the fission products with the following atomic numbers: Z = 30, 31, 32, 33, 34, 35, 37, 38, 39, 40, 48, 49, 50, 53, 55, 56, 57, 58, 59, 60, 61, 62, 63, 64, 65, 66, 67, 68, 69 and 70. The fertile blanket is

reprocessed at a rate of 40 L per day to continuously extract actinides and reinject them into the fuel salt. Additionally, the fission products in the blanket are removed at a rate of 0.4 L per day. The MSFR burnup calculation is performed with four depletion cells defined, representing the core, loop, reprocessing plant, and fertile blanket, respectively. In this regard, the MSFR pumps, heat exchangers, and piping are treated together in the loop cell. The volume of the reprocessing plant is set to be 40 L, which corresponds to a holdup time of one day. The removal elements and their corresponding removal rates of the elements at each depletion cell are summarized in Table 6. It is important to note that the reprocessing throughputs and element-wise removal fractions are adopted from Ref. [29] and are intended as illustrative example inputs to demonstrate the modeling workflow, rather than as validated or optimized design parameters.

Table 5. The material composition and density in MSFR.

Material	Molar Fraction				Density [g/cm^3]
Fuel salt	Li-6	1.45×10^{-5}	U-233	0.009402	4.1249
	Li-7	0.289705	F-19	0.626168	
	Th-232	0.07471			
Fertile blanket	Li-6	1.45×10^{-5}	Th-232	0.084112	4.1249
	Li-7	0.289705	F-19	0.626168	
B_4C	C-12	0.19778	B-10	0.15840	2.52
	C-12	0.00222	B-11	0.64160	
Ni-based alloy	Ni	0.79432	Mn	0.00257	10.0
	W	0.09976	Si	0.00252	
	Cr	0.08014	Al	0.00052	
	Mo	0.00736	B	0.00033	
	Fe	0.00632	P	0.00023	
	Ti	0.00295	S	0.00003	
	C	0.00294			

Table 6. The removal rates of elements at various depletion cells for the MSFR.

Depletion Cell	Elements	Removal Rate [s^{-1}]	Volume [L]
Core	H, He, N, O, Ne, Ar, Kr, Nb, Mo, Tc, Ru, Rh, Pd, Ag, Sb, Te, Xe, Rn	2.31×10^{-2}	9005.9
Loop	-	-	8971.5
Reprocessing plant	Zn, Ga, Ge, As, Se, Br, Rb, Sr, Y, Zr, Cd, In, Sn, I, Cs, Ba, La, Ce, Pr, Nd, Pm, Sm, Eu, Gd, Tb, Dy, Ho, Er, Tm, Yb	1.1574×10^{-4}	40.0
Fertile blanket	H, He, N, O, Ne, Ar, Kr, Nb, Mo, Tc, Ru, Rh, Pd, Ag, Sb, Te, Xe, Rn	2.31×10^{-2}	7325.7
	Zn, Ga, Ge, As, Se, Br, Rb, Sr, Y, Zr, Cd, In, Sn, I, Cs, Ba, La, Ce, Pr, Nd, Pm, Sm, Eu, Gd, Tb, Dy, Ho, Er, Tm, Yb	6.3197×10^{-10}	
	U, Np, Pu, Am, Cm, Bk, Cf, Es, Fm, Md, No, Lr	6.3197×10^{-8} (Reinjected into the core)	

The design power of the MSFR is 3 GWth. However, it is not stated in the MSFR benchmark specification whether this power is used as normalization for the burnup calculation. As shown later, at this power level the rector cannot reach equilibrium, contrary to the expectation of the benchmark developers. In fact, the reactor composition evolution reported in the benchmark study [29] matches the results obtained under the assumption of constant flux normalization, as discussed in Ref. [30]. Due to this reason, two sets of depletion calculations are conducted in the MSFR application. The first set assumes constant

power of 3 GW, while the second set assumes constant average flux of 3.5×10^{15} $cm^{-2}s^{-1}$, which is the normalization factor suggested in Ref. [30].

5.2. Simulation Results

Using the developed multi-point depletion model, the MSFR burnup calculation was carried out under two normalization conditions: one assumes the constant power and the other assumes the constant average flux throughout the core. The constant power case continued until the system no longer contained sufficient fissile materials to sustain operation. The constant flux case, by contrast, was extended to a total duration of 200 years. In both scenarios, the maximum micro-step size was set to be one year.

Figure 11 compares the evolutions of the k_{eff} value and fission power obtained from the burnup calculations under the two normalization conditions. Because the simulation started from the critical inventory, the k_{eff} significantly dropped below unity right after the start of the simulation. In actual operation, the starting composition is expected to provide excess reactivity. The k_{eff} at the constant power condition recovers faster than that at the constant flux condition, indicating a higher rate of uranium production. On the other hand, the power generated at the constant flux condition is much lower than that of the constant power condition, indicating a lower burnup rate under that condition.

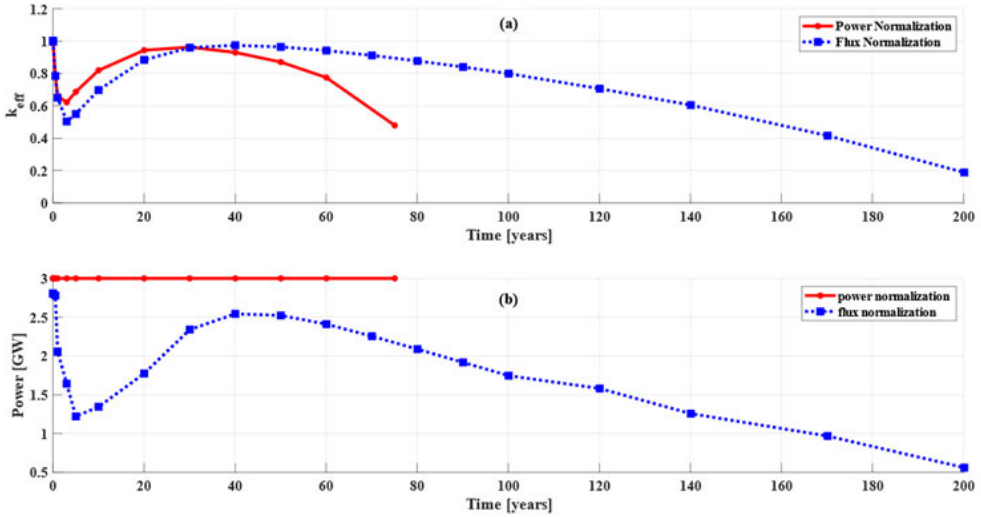

Figure 11. Comparison of (**a**) k_{eff} and (**b**) power evolutions under two normalization conditions.

The evolutions of the inventories of Th-232, uranium, and TRU elements are shown in Figures 12–14, respectively. Regardless of the normalization condition, the inventory of Th-232 gradually decreases as it is converted to U-233. The consumption rate of Th-232 in the constant power case is significantly higher compared to the constant flux case. At the beginning stage of the burnup sequence, the U inventory drops sharply, followed by a steady increase that surpasses its initial level. This is driven by the transmutation of Th-233 and the recycling of actinides from the blanket to the salt fuel. Towards the end of the burnup, the uranium inventory declines rapidly because both blanket and fuel salt essentially contain only depleted Th-232 by that time. The inventories of TRU elements increase steadily over time, with a notably higher growth rate observed in the constant power case.

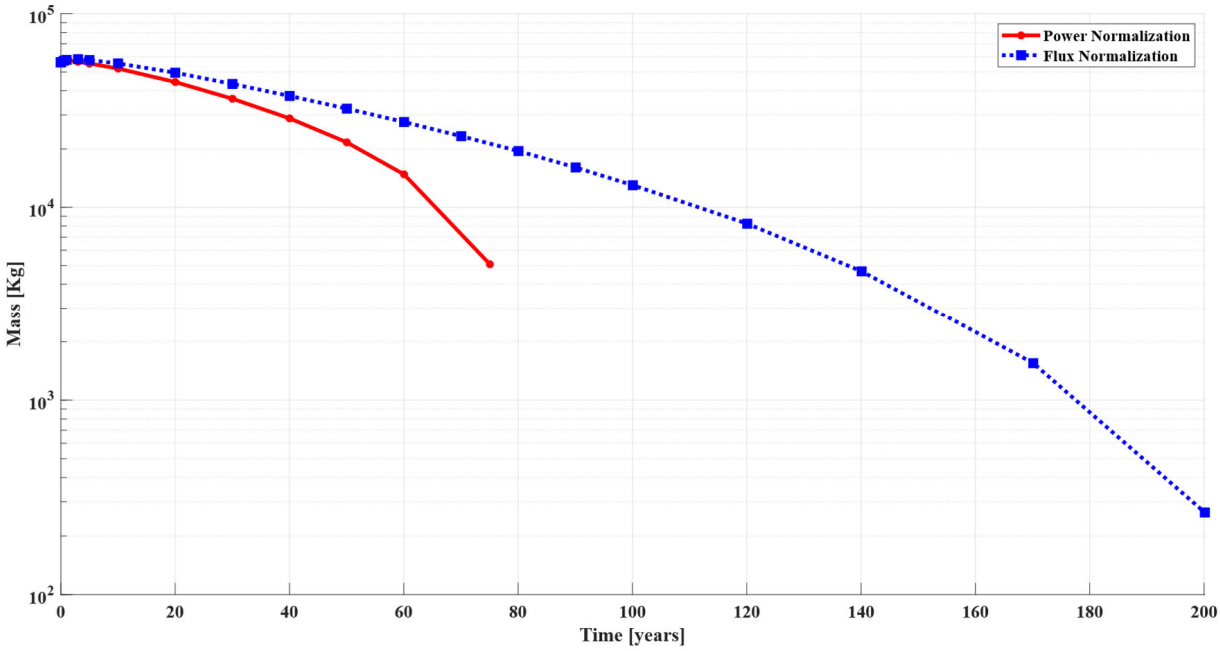

Figure 12. Evolution of the total mass of Th-232 in the MSFR.

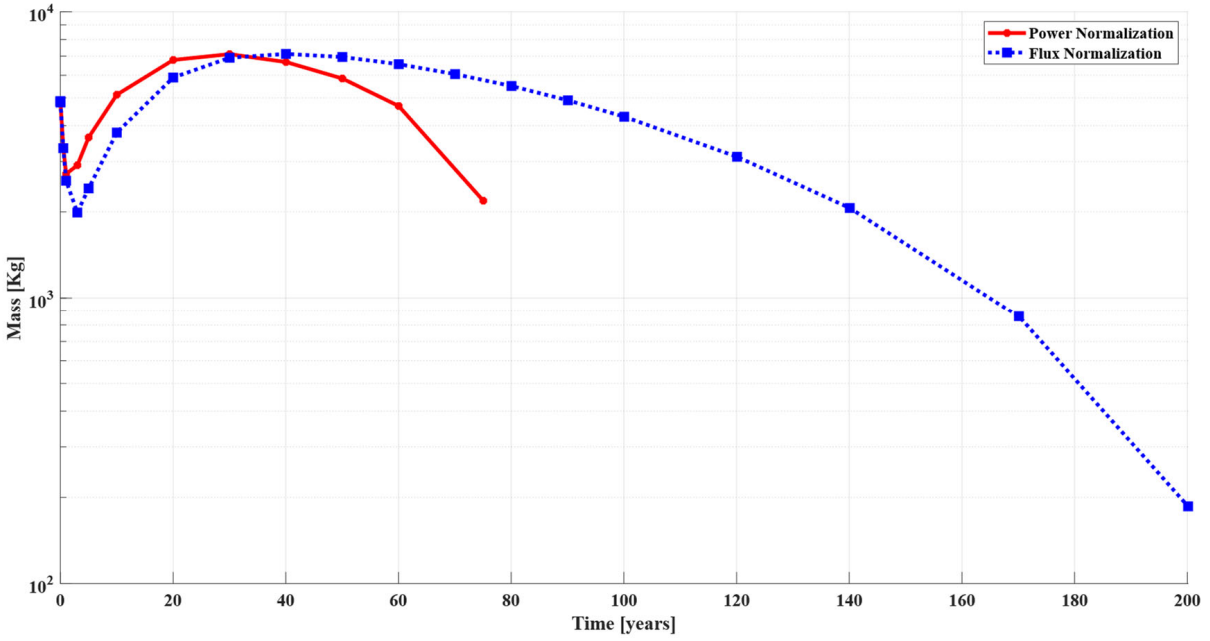

Figure 13. Evolution of total mass of uranium in the MSFR.

Due to the unspecified normalization condition used in the benchmark, a direct comparison between the current results and the benchmark data is not possible due to the unspecified normalization condition. Nevertheless, it is evident that neither of the normalization conditions adopted in this study led to identical steady-state results as indicated by the benchmark study [29]. This implies that the benchmark likely did not assume the designed thermal power of the reactor as the normalization basis, but instead used a constant neutron flux level, most likely lower than 3.5×10^{15} $cm^{-2}s^{-1}$, to allow the system to reach equilibrium under the proposed reprocessing scheme.

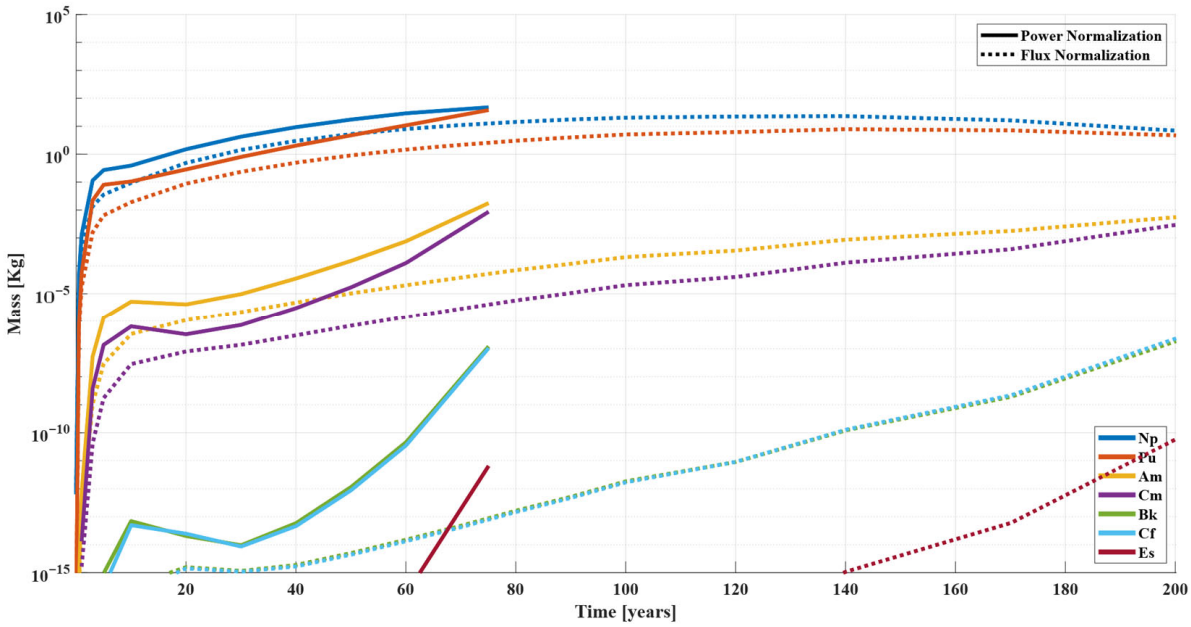

Figure 14. Evolution of total mass of TRU elements in the MSFR.

Finally, the evolution of some representative fission products is shown in Figure 15. In general, the fission product inventory reached equilibrium quickly. All fission products are either gases or originate from gaseous precursors. The removal of these fission products through the off-gas system and the reprocessing plant helps maintain their concentrations within low limits.

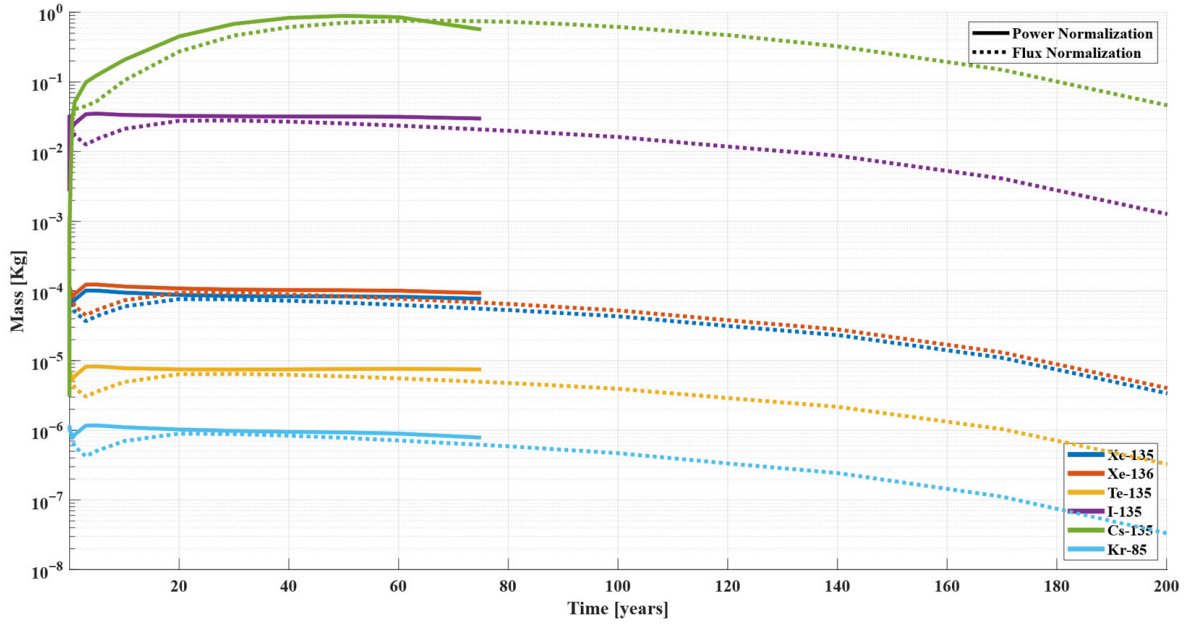

Figure 15. The evolution of six major fission products in the MSFR.

5.3. A New Reprocessing Scheme

Since the depletion of Th-232 was the primary factor limiting the MSFR from reaching equilibrium operation, a slightly modified reprocessing scheme was proposed to expedite the achievement of steady-state operation. The new scheme is nearly the same as the one described in Section 5.1 except a different reprocessing strategy is implemented to the blanket. Instead of extracting actinides from the blanket salt at a rate of 40 L per day, the

new strategy removes the blanket salt at the same rate but replaces it with fresh fertile salt with initial material composition. In this modified scheme, all actinides in the removed salt are still recovered and reinjected into the core. Simultaneously, an external source of fresh fertile salt is added to the blanket to replenish the depleted Th-232.

With the new reprocessing scheme, the depletion calculation is performed, assuming a constant power of 3 GW for a duration of 200 years. The maximum micro-step is again set to be one year. The evolution of heavy metals under the new reprocessing scheme is shown in Figure 16. The results indicate that the system rapidly reached equilibrium, with uranium isotopes reaching equilibrium after about three years.

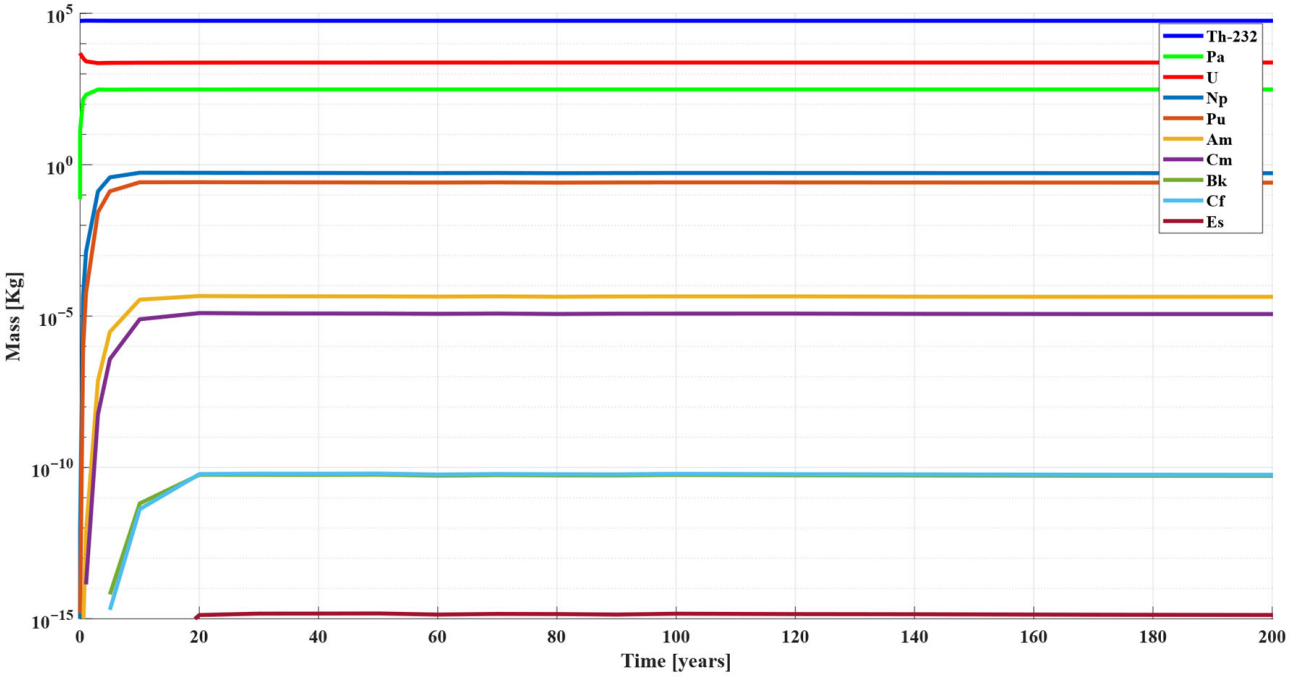

Figure 16. Evolution of heavy metals in the MSFR under the new reprocessing scheme.

To further explore the materials distribution among various components under the new reprocessing scheme, the concentration of Th-232 and U-233 in both the fuel salt and blanket salt are shown in Figures 17 and 18 respectively. As shown in Figure 17, in the core region, the concentration of Th-232 in the fuel salt initially increases due to the accumulation of Pa-231, which captures neutrons and quickly forms Pa-232. The unstable Pa-232 subsequently undergoes beta decay (with a half-life of approximately 1.3 days) to produce U-232. In the blanket region, Th-232 initially decreases as it undergoes neutron capture and transmutation. However, this decline is short-lived, as the fresh fertile salt feed stream replenishes the depleted material, allowing the concentration to stabilize and reach equilibrium in a short time. For U-233, as shown in Figure 18, its concentration in the blanket salt initially increases over time and reaches equilibrium as actinides are extracted and recycled back to the core. In contrast, the concentration of U-233 in the fuel salt initially drops due to the consumption in fission reactions. It eventually stabilizes as well, supported by the continuous recovery and reinjection of actinides from the blanket salt.

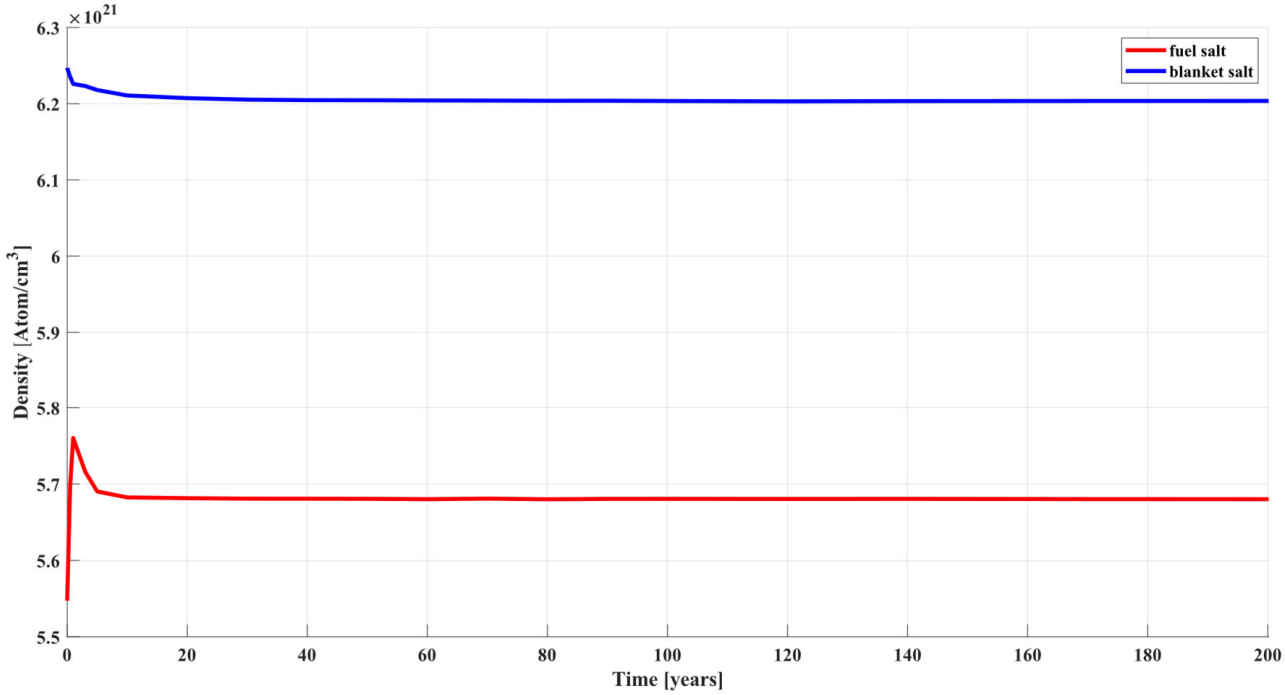

Figure 17. Evolution of the concentration of Th-232 in the fuel and blanket salts.

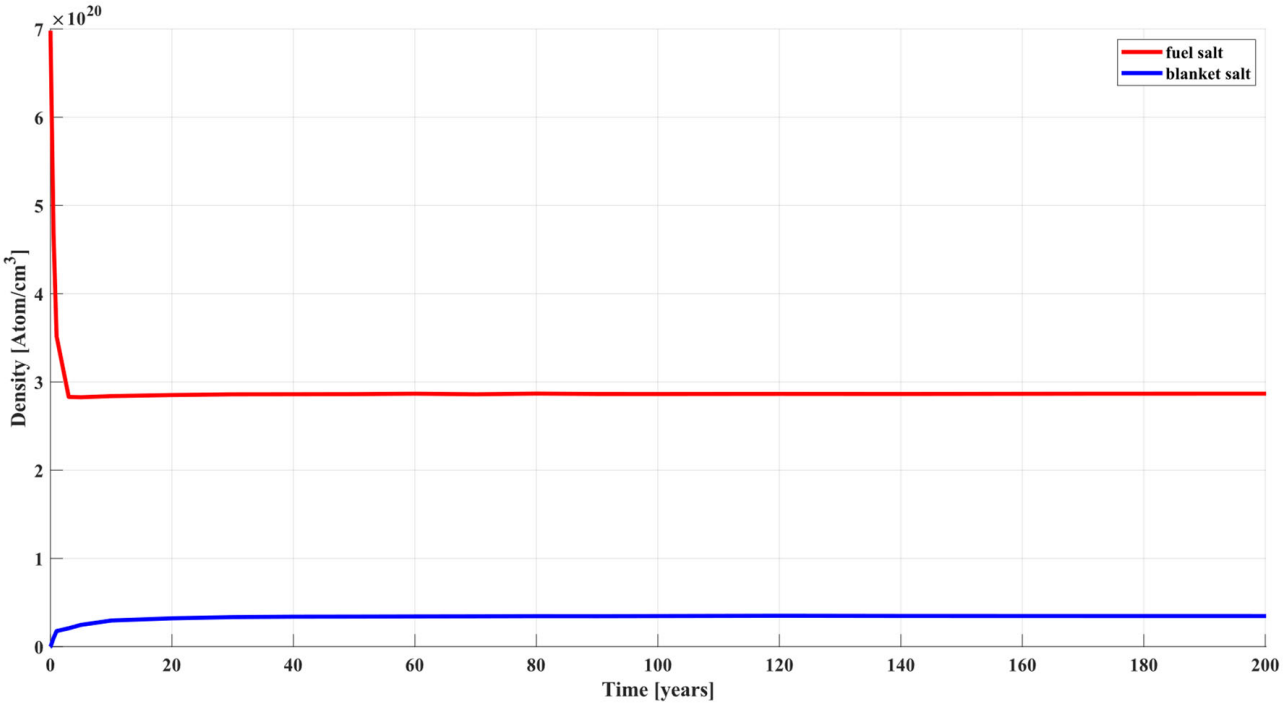

Figure 18. Evolution of the concentration of U-233 in the fuel and blanket salts.

The distributions of various fission products across the reactor components under the new reprocessing scheme are shown in Figure 19. The concentration of fission products reaches equilibrium after approximately three years of operation. In the blanket region, the fission product is negligible due to the low fission rate, removal via the off-gas system, and removal through displacement by the fresh fertile salt feed stream. In the core region, the equilibrium concentration of each isotope varies depending on the reaction dynamics. Gaseous fission products are most concentrated in the reprocessing cell since it is not connected to the off-gas system. The concentration of Te-135 is highest in the core, lower

in the loop, and minimal in the reprocessing cell. This results from its very short half-life of 19 s, causing it to decay almost instantaneously. The concentrations of I-135 (half-life: 6.6 h) and Cs-135 (half-life: 2.3×10^6 years) are nearly identical in the core and loop region because their decay rates are slow compared to the fuel circulation rate. Their concentrations in the reprocessing cell are minimal due to continuous removal.

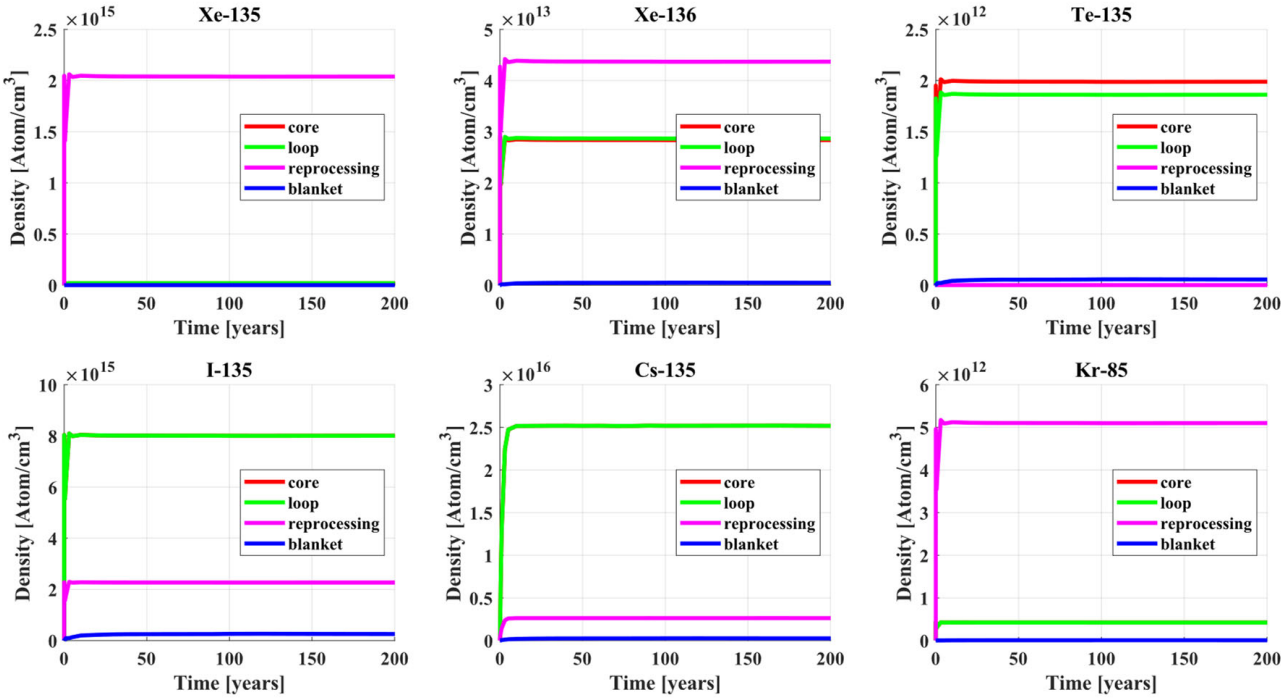

Figure 19. Evolution of the concentration of fission products in different depletion cells.

6. Conclusions

In this work, we develop a novel multi-point depletion model specifically designed for burnup calculations in circulating-fuel systems such as MSRs. The model employs a finite-volume framework to represent depletion cells and applies continuity equations to capture mass flow between them. The resulting changes in isotopic concentration from the circulating flow are incorporated directly into the Bateman equation for burnup calculations. This approach removes the need for advection-based mass transport models and avoids the numerical instabilities associated with coarse spatial discretization.

The proposed approach yields a system of coupled linear ODEs that can be solved efficiently using advanced linear algebra techniques. All depletion cells are assembled into a fully coupled system matrix. Additional flow-dependent processes such as noble gas volatilization, noble metal deposition, and fuel reprocessing are incorporated as sink terms using user-specified removal rates, while external feeds (e.g., fresh fertile salt or specific isotopic injections) enter as independent source terms. Overall, this method provides a mid-fidelity capability for MSR burnup analysis, bridging the gap between point-depletion models and fully resolved spatiotemporal treatments, which are often computationally prohibitive for tracking numerous isotopes over long timescales.

The developed model is implemented in the open-source depletion code ONIX, leveraging its interface with the Monte Carlo transport code OpenMC. The new module provides a flexible framework for defining depletion cells and modeling flow-dependent phenomena. It automatically constructs a connectivity matrix encoding mass transfer and reaction rates between cells. For each cell, OpenMC generates the conventional depletion matrix, which is inserted into the diagonal band of the global connectivity matrix to form the complete

system matrix for depletion. This matrix is solved using the CRAM on a fine time grid (micro-steps), while the depletion matrices from OpenMC are updated on a coarser time grid (macro-steps). The module also allows normalization by either constant power or constant neutron flux condition and supports tracking radioactivity in gas holdup tanks and deposition surfaces.

The module was validated using an MSRE-based benchmark. The computed isotopic inventories showed strong agreement with experimental data for salt-seeking isotopes and those without noble-gas precursors. For most other isotopes, the model tended to overpredict inventories, indicating that the benchmark's assumed removal rates may be underestimated. The model was further applied to one reference MSFR design, and a new reprocessing scheme enabling faster steady-state operation was proposed, involving continuous fertile salt feed to the blanket and recycling of actinides back into the core. Future extensions of the model will include built-in representations of mass transfer between the fluid and gas phases and between the fluid and solid surfaces. This will eliminate the need for user-defined removal rates and enable more accurate predictions of flow-dependent phenomena. Additionally, a dedicated parallel performance and scaling study, particularly for larger numbers of loop regions and tracked isotopes, is planned as future work.

Author Contributions: M.H.E. conceptualization, methodology, software, investigation, data curation, formal analysis, visualization, writing—original draft. Z.W. Conceptualization, supervision, funding acquisition, validation, writing—review & editing. All authors have read and agreed to the published version of the manuscript.

Funding: This work is partially supported by the U.S. DOE Nuclear Energy University Program with the Award No. DE-NE0009162.

Data Availability Statement: All data and associated software developed in this project will be made publicly available through a GitHub repository (https://github.com/Mhelhareef/ONIX/tree/MSR accessed on 9 February 2026).

Acknowledgments: The authors thank Tingzhou Fie at Argonne National Laboratory for providing the MSRE OpenMC model and insightful discussions along with the manuscript preparation. The authors also acknowledge the College of Engineering at the Virginia Commonwealth University for providing high-performance computing resources that have contributed to the research results reported in this paper.

Conflicts of Interest: The authors declare no conflicts of interest.

References

1. Robertson, R.C. *Conceptual Design Study of a Single-Fluid Molten-Salt Breeder Reactor*; No. ORNL-4541. comp.; Oak Ridge National Lab (ORNL): Oak Ridge, TN, USA, 1971.
2. LeBlanc, D. Molten salt reactors: A new beginning for an old idea. *Nucl. Eng. Des.* **2010**, *240*, 1644–1656. [CrossRef]
3. Delpech, S.; Merle-Lucotte, E.; Heuer, D.; Allibert, M.; Ghetta, V.; Le-Brun, C.; Doligez, X.; Picard, G. Reactor physic and reprocessing scheme for innovative molten salt reactor system. *J. Fluor. Chem.* **2009**, *130*, 11–17. [CrossRef]
4. Serp, J.; Allibert, M.; Beneš, O.; Delpech, S.; Feynberg, O.; Ghetta, V.; Heuer, D.; Holcomb, D.; Ignatiev, V.; Kloosterman, J.L.; et al. The molten salt reactor (MSR) in generation IV: Overview and perspectives. *Prog. Nucl. Energy* **2014**, *77*, 308–319. [CrossRef]
5. Gérardin, D.; Allibert, M.; Heuer, D.; Laureau, A.; Merle-Lucotte, E.; Seuvre, C. Design evolutions of the molten salt fast reactor. In Proceedings of the International Conference on Fast Reactors and Related Fuel Cycles: Next Generation Nuclear Systems for Sustainable Development (FR17) Programme and Papers, (p. v), Yekaterinburg, Russia, 26–29 June 2017; International Atomic Energy Agency (IAEA): Vienna, Austria, 2017.
6. Betzler, B. *Liquid-Fueled Molten Salt Reactor Depletion Modeling*; Oak Ridge National Laboratory: Oak Ridge, TN, USA, 2021.
7. Walker, S.A.; Tano, M.E.; Abou-Jaoude, A.; Calvin, O. Depletion-driven thermochemistry of molten salt reactors: Review, method, and analysis. *Front. Nucl. Eng.* **2023**, *2*, 1214727. [CrossRef]
8. Aufiero, M.; Cammi, A.; Fiorina, C.; Leppänen, J.; Luzzi, L.; Ricotti, M. An extended version of the SERPENT-2 code to investigate fuel burn-up and core material evolution of the Molten Salt Fast Reactor. *J. Nucl. Mater.* **2013**, *441*, 473–486. [CrossRef]

9. Hartanto, D.; Bostelmann, F.; Betzler, B.R.; Bekar, K.B.; Hart, S.W.; Wieselquist, W.A. SCALE depletion capabilities for molten salt reactors and other liquid-fueled systems. *Ann. Nucl. Energy* **2023**, *196*, 110236. [CrossRef]
10. Nelson, A.G.; Jarrett, M.G.; Chee, G.J.Y. Molten salt reactor depletion techniques in the ADDER reactor depletion and fuel management analysis core. In Proceedings of the International Conference on Mathematics and Computational Methods Applied to Nuclear Science and Engineering-M&C 2021, Oak Ridge, TN, USA, 3–7 October 2021.
11. de Troullioud de Lanversin, J.; Kütt, M.; Glaser, A. ONIX: An open-source depletion code. *Ann. Nucl. Energy* **2021**, *151*, 107903. [CrossRef]
12. Romano, P.K.; Horelik, N.E.; Herman, B.R.; Nelson, A.G.; Forget, B.; Smith, K. OpenMC: A state-of-the-art Monte Carlo code for research and development. *Ann. Nucl. Energy* **2015**, *82*, 90–97. [CrossRef]
13. Elhareef, M. ONIX-MSR: Extended ONIX Version with Circulating-Fuel Depletion Capability. GitHub. Available online: https://github.com/Mhelhareef/ONIX/tree/MSR (accessed on 9 February 2026).
14. Fei, T.; Shahbazi, S.; Hartanto, D.; Davidson, E.; Walker, S.; Tano, M. Demonstration and preliminary validation of Griffin for MSR depletion with chemical removal parametric studies. *Trans. Am. Nucl. Soc.* **2025**, *132*, 958–961.
15. Seifert, L.; Shahbazi, S.; Richards, S.; Munk, M.; Huff, K. Accuracy of the Scaled Flux Method for Spatially Resolved Nuclide Transmutation in Flowing-Fuel Molten Salt Reactors. *Nucl. Sci. Eng.* **2025**, 1–13. [CrossRef]
16. Zhang, Y.; Zou, Y.; Yan, R.; Zhu, G.; Zhang, Q. A comprehensive depletion code MACT for molten salt reactors. *Ann. Nucl. Energy* **2025**, *224*, 111709. [CrossRef]
17. Elhareef, M.; Yim, M.S. Use of Optimal Detection of Changepoints to Support Near Real-Time Nuclear Accountancy of Advanced Nuclear Reactors. In Proceedings of the ANS Winter Meeting, Washington, DC, USA, 9–12 November 2025.
18. Cetnar, J. General solution of Bateman equations for nuclear transmutations. *Ann. Nucl. Energy* **2006**, *33*, 640–645. [CrossRef]
19. Maria, P. Higher-Order Chebyshev Rational Approximation Method and Application to Burnup Equations. *Nucl. Sci. Eng.* **2016**, *182*, 297–318. [CrossRef]
20. Brown, D.; Chadwick, M.; Capote, R.; Kahler, A.; Trkov, A.; Herman, M.; Sonzogni, A.; Danon, Y.; Carlson, A.; Dunn, M.; et al. ENDF/B-VIII.0: The 8 th Major Release of the Nuclear Reaction Data Library with CIELO-project Cross Sections, New Standards and Thermal Scattering Data. *Nucl. Data Sheets* **2018**, *148*, 1–142. [CrossRef]
21. Harris, C.R.; Millman, K.J.; van der Walt, S.J.; Gommers, R.; Virtanen, P.; Cournapeau, D.; Wieser, E.; Taylor, J.; Berg, S.; Smith, N.J.; et al. Array programming with NumPy. *Nature* **2020**, *585*, 357–362. [CrossRef] [PubMed]
22. Gabbard, C.H. *Reactor Power Measurement and Heat Transfer Performance in the Molten Salt Reactor Experiment*; ORNL-TM-3002; Oak Ridge National Laboratory: Oak Ridge, TN, USA, 1970.
23. Robertson, R.C. *MSRE Design & Operations Report Part 1 Description of Reactor Design*; ORNL-TM-728; Oak Ridge National Laboratory: Oak Ridge, TN, USA, 1965.
24. Fratoni, M.; Shen, D.; Ilas, G.; Powers, J. *Molten Salt Reactor Experiment Benchmark Evaluation*; DOE-UCB-8542; University of California: Berkeley, CA, USA; Oak Ridge National Laboratory: Oak Ridge, TN, USA, 2020.
25. Elhareef, M.; Wu, Z. Benchmarking a point reactor kinetics method with delayed neutron precursors transport using data from molten salt reactor experiment. *Ann. Nucl. Energy* **2025**, *217*, 111366. [CrossRef]
26. Elhareef, M.; Abouhussien, Y.; Wu, Z.; Fratoni, M.; Davidson, E.; Fei, T.; Harris, K. A Reactor Transient Benchmark for Molten Salt Reactor Experiment Pump Transient Tests. *Nucl. Sci. Eng.* **2025**, *199*, 2143–2171. [CrossRef]
27. Compere, E.L.; Kirslis, S.; Bohlmann, E.; Blankenship, F.; Grimes, W. *Fission Product Behavior in the Molten Salt Reactor Experiment*; ORNL-4856; Oak Ridge National Laboratory: Oak Ridge, TN, USA, 1975. [CrossRef]
28. Fei, T.; Shahbazi, S.; Fang, J.; Shaver, D. *Validation of NEAMS Tools Using MSRE Data*; No. ANL/NSE-22/48; Argonne National Laboratory: Argonne, IL, USA, 2022.
29. Brovchenko, M.; Kloosterman, J.-L.; Luzzi, L.; Merle, E.; Heuer, D.; Laureau, A.; Feynberg, O.; Ignatiev, V.; Aufiero, M.; Cammi, A.; et al. Neutronic benchmark of the molten salt fast reactor in the frame of the EVOL and MARS collaborative projects. *EPJ Nucl. Sci. Technol.* **2019**, *5*, 2. [CrossRef]
30. Pauwels, F. Burnup Simulations of the Thorium Cycle in a MSFR Using Perturbation Theory. Master Thesis, Delft University of Technology, Delft, The Netherlands, 2020.